HHS Public Access

Author manuscript

ACS Chem Neurosci. Author manuscript; available in PMC 2017 December 20.

Published in final edited form as:

ACS Chem Neurosci. 2017 September 20; 8(9): 1937–1948. doi:10.1021/acschemneuro.7b00098.

Synthesis and preliminary studies of a novel negative allosteric modulator [^{11}C]QCA for imaging of metabotropic glutamate receptor 2

Xiaofei Zhang[†,¶,#], **Katsushi Kumata**[‡,#], **Tomoteru Yamasaki**[‡], **Ran Cheng**[†], **Akiko Hatori**[‡], **Longle Ma**[†], **Yiding Zhang**[‡], **Lin Xie**[‡], **Lu Wang**[†], **Hye Jin Kang**[⊥], **Douglas J. Sheffler**[§], **Nicholas D. P. Cosford**[§], **Ming-Rong Zhang**[*,‡], and **Steven H. Liang**[*,†]

[†]Nuclear Medicine and Molecular Imaging, Massachusetts General Hospital & Department of Radiology, Harvard Medical School, Boston, MA, 02114, USA

[¶]State Key Laboratory and Institute of Elemento-Organic Chemistry, Collaborative Innovation Center of Chemical Science and Engineering, Nankai Unviersity, Tianjin 300071, China

[‡]Department of Radiopharmaceutics Development, National Institute of Radiological Sciences, National Institutes for Quantum and Radiological Science and Technology, Chiba, 263-8555, Japan

[⊥]Department of Pharmacology & National Institute of Mental Health Psychoactive Drug Screening Program, University of North Carolina at Chapel Hill, North Carolina, 27515, USA

[§]Cell Death and Survival Networks Program and Conrad Prebys Center for Chemical Genomics, Sanford-Burnham Medical Research Institute, La Jolla, CA, 92037, USA

Abstract

Metabotropic glutamate 2 receptors ($mGlu_2$) are involved in the pathogenesis of several CNS disorders and neurodegenerative diseases. Pharmacological modulation of this target represents a potential disease-modifying approach for the treatment of substance abuse, depression, schizophrenia and dementias. While quantification of $mGlu_2$ receptors in the living brain by positron emission tomography (PET) would help us better understand signaling pathways relevant to these conditions, few successful examples have been demonstrated to image $mGlu_2$ in vivo and a suitable PET tracer is yet to be identified. Herein we report the design and synthesis of a radiolabeled negative allosteric modulator (NAM) for $mGlu_2$ PET tracer development based on a quinoline 2-carboxamide scaffold. The most promising candidate, 7-((2,5-dioxopyrrolidin-1-yl)methyl)-4-(2-fluoro-4-[^{11}C]methoxyphenyl) quinoline-2-carboxamide ([^{11}C]QCA) was

[*]**Corresponding Author**. Tel: +81 433 823 709. Fax: +81-43-206-3261. zhang.ming-rong@qst.go.jp. Tel: +1 617 726 6107. Fax: +1 617 726 6165. liang.steven@mgh.harvard.edu.

[#]These authors contribute equally to this work.

ASSOCIATED CONTENT

Retrosynthetic analysis; Characterization of all new compounds and NMR spectra; assay methods; GPCRome data sheet. This material is available free of charge via the Internet at http://pubs.acs.org.

Author Contributions

The manuscript was written through contributions of all authors. All authors have given approval to the final version of the manuscript. [#]X. Zhang and K. Kumata contributed equally.

The authors declare no competing financial interest.

prepared in 13% radiochemical yield (non-decay corrected at the end of synthesis) with >99% radiochemical purity and >74 GBq/μmol (2 Ci/μmol) specific activity. While the tracer showed limited brain uptake (0.3 SUV), probably attributable to effects on PgP/Bcrp efflux pump, in vitro autoradiography studies demonstrated heterogeneous brain distribution and specific binding. Thus, [^{11}C]QCA is a chemical probe that provides the basis for the development of a new generation $mGlu_2$ PET tracers.

Graphical abstract

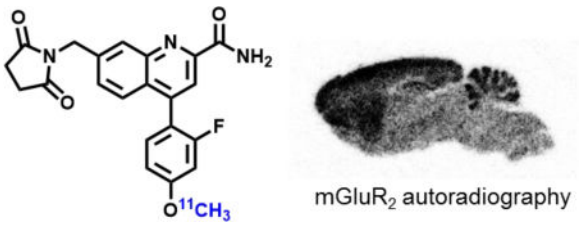

Keywords

positron emission tomography; metabotropic glutamate receptor 2; $mGlu_2$; ^{11}C; negative allosteric modulator

INTRODUCTION

Glutamate is the most abundant endogenous excitatory neurotransmitter and glutamate receptors (Glus) play a pivotal role in modulating a wide scope of neurological functions in the central nervous system (CNS).[1–6] Glutamatergic signaling is primarily mediated via two distinct groups, namely ionotropic receptors (iGlus) and the G protein-coupled metabotropic receptors (mGlus). Based on different sequence homology, anatomical distribution and pharmacology, the mGlus are typically divided into three subcategories. Group I mGlus ($mGlu_1$ and $mGlu_5$), coupled to G_q/G_{11} proteins, mobilize calcium from intracellular stores upon activation and increase protein kinase C activity. Group II ($mGlu_2$ and $mGlu_3$) and Group III ($mGlu_4$, $mGlu_6$, $mGlu_7$ and $mGlu_8$) mGlus, coupled to $G_{i/o}$ proteins, downregulate cAMP formation through inhibition of adenylyl cyclase.[7] In particular, $mGlu_2$ receptors negatively regulate endogenous glutamate release and consequently may be involved in the protection of neurons against excitotoxicity. The receptors are predominantly localized on presynaptic membranes although they are also found in peripheral regions of the synapse.[8,9] Moderate-to-high expression of $mGlu_2$ can be found in many brain regions, including the cerebral cortex, cerebellum, amygdala and hippocampus.[10–14] It has been reported that $mGlu_2$ is involved in the pathogenesis of numerous brain dysfunctions, including psychiatric disorders and neurodegenerative diseases.[7,15–19] Therefore pharmacological modulation of $mGlu_2$ represents a promising therapeutic approach for the treatment of several CNS diseases,[20] including drug dependence,[21–23] chronic pain,[24] anxiety,[17] depression,[25,26] schizophrenia,[27] Parkinson's disease[28,29] and Alzheimer's disease.[30] Initial drug discovery efforts focused on non-selective $mGlu_{2/3}$ agonists and antagonists that bind to the mGlu orthosteric binding site (evolutionarily conserved glutamate binding site);[31] however, in recent years there has been a shift towards allosteric modulation strategies (consisting of

positive and negative allosteric modulators; abbreviated as PAM and NAM, respectively) that offer the potential for improved selectivity for $mGlu_2$ or $mGlu_3$.[32,33] While a wide range of highly selective $mGlu_2$ PAMs have been discovered and recently reviewed,[33,34] the development of selective $mGlu_2$ NAMs has remained in its nascent stage with only one report based on a dihydroquinoline 2-carboxamide scaffold in the primary literature.[35]

Positron emission tomography (PET) is a non-invasive imaging technology that is capable of quantifying biochemical processes in vivo,[36–39] which would enable investigations of $mGlu_2$ based glutamatergic signaling under normal and disease conditions, and assessment of distribution and testing target engagement and dose occupancy of $mGlu_2$ drug candidates for clinical trials. Unlike several $mGlu_1$ or $mGlu_5$-targeting PET radiotracers in human use,[40–45] there is an unmet need for probing $mGlu_2$ in clinical research and drug development towards this important receptor subtype in the glutamatergic pathway. As shown in Figure 1, there are continuous research efforts in the development of $mGlu_2$ PET tracers,[40–43] including [^{11}C]CMGDE (**1**),[46,47] [^{11}C]JNJ-42491293 (**2**),[48,49] [^{18}F]FE-JNJ42491293 (**3**),[50] [^{11}C]CMDC (**4**)[51] and two tracers (^{18}F-compound **5** and ^{11}C-compound **6**) in the patent literature.[52,53] Among these studies [^{11}C]CMGDE (**1**), the first $mGlu_2$ radiotracer based on a prodrug of an antagonist LY341495, provided a foundation for the further development of a specific $mGlu_2$ tracer.[47] On the other hand [^{11}C]CMDC (**4**), a derivative of JNJ-40068782,[54] was not further pursued due to limited brain penetration (peak brain uptake *ca.* 0.6 SUV).[51] Preliminary evaluation in PET imaging studies for compounds **3**, **5**, **6** are not yet disclosed for the development of $mGlu_2$ tracers.[52,53] Only two PET tracers, namely [^{11}C]JNJ-42491293 (**2**) and a ^{11}C-compound from Merck, have been advanced to first-in-human studies. [^{11}C]JNJ-42491293 (**2**) was discontinued for $mGlu_2$ imaging due to unexpected off-target binding in vivo during clinical trials[55,56] and only limited preliminary data on the Merck compound (no structural information) were reported in abstracts.[57,58] These $mGlu_2$ imaging efforts combined with pharmaceutical development and the potential of $mGlu_2$-modulating pharmacotherapy provide a strong impetus to advance PET tracer development for this target.

Herein we describe the synthesis of a small array of potent and selective $mGlu_2$ NAMs that are amenable for radiolabeling and their preliminary evaluation in rodents by PET. In vitro autoradiography studies confirm the specific binding of these new NAMs bearing a quinoline 2-carboxamide moiety, which provides an excellent starting point for future $mGlu_2$ PET tracer design.

RESULTS AND DISCUSSION

Chemistry

We designed a focused library of small molecule based on a series of NAMs disclosed in the patent literature,[59] with the goal to develop a selective $mGlu_2$ PET tracer amenable to radiolabeling with either ^{11}C or ^{18}F. In particular, the succinimidyl compound **16** was selected in our proof-of-concept studies because of reported low EC_{50} value (8 nM), reasonable cLogP value (2.95) and amenability for ^{11}C-labeling from its corresponding phenolic precursor. Thus a set of quinolone 2-carboxamides and their labeling precursors were synthesized according to our synthetic strategy (see detailed retrosynthetic analysis in

Scheme S1 of Supporting Information, SI). As summarized in Scheme 1, oxidation of 7-methylquinoline (**7**) with *m*CPBA followed by cyanide addition provided quinoline-2-carbonitrile **8** in 74% yield over two steps, which was converted to chloroquinoline **9** after *m*CPBA oxidation and $POCl_3$ chlorination (60% yield). Site-specific bromination at the benzyl position of chloroquinoline **9** followed by succinimide substitution gave key intermediate **11** in 80% yield. Several parallel syntheses were carried out to introduce aryl groups at the ipso position of the chloride via palladium catalyzed Suzuki cross-coupling reactions. The coupling reaction with (2-fluoro-4-methoxyphenyl)boronic acid gave quinoline nitrile **12**, which was hydrolyzed in basic H_2O_2 solution to afford the final standard 7-((2,5-dioxopyrrolidin-1-yl)methyl)-4-(2-fluoro-4-methoxyphenyl)quinoline-2-carboxamide (QCA; **16**) in 55% yield over 2 steps. The cross coupling procedure was also applied to obtain phenol **17** (51% yield), fluoroethyl (FEPAD (**18**), 60% yield) and fluoropropyl derivatives (FPPAD (**19**), 53% yield). In brief, the synthesis of QCA (**16**), its precursor **17** and fluorinated derivatives (**18**–**19**) were achieved in eight to nine steps with overall yields of 6% - 10%.

Pharmacology and physicochemical properties

QCA and its two fluorinated derivatives (FEQCA and FPQCA) were subsequently screened for their *in vitro* activity towards $mGlu_2$ and $mGlu_3$, and the results are shown in Figure 2. A thallium flux assay in human embryonic kidney 293 (HEK) cells expressing heteromeric G-protein coupled inwardly rectifying potassium (GIRK) channels[60] and human $mGlu_2$ or $mGlu_3$, was utilized to determine potency, efficacy and selectivity. The concentration-response relationship that antagonizes the effect of an EC_{80} concentration of glutamate was determined for each candidate. Potency is expressed as the IC_{50} for inhibition of the glutamate EC_{80} response. All three candidates showed NAM activity (IC_{50} values 45 ± 5 nM for QCA, 130 ± 10 nM for FEQCA, and 1080 ± 1300 nM for FPQCA) at human $mGlu_2$ and excellent selectivity for $mGlu_2$ over $mGlu_3$. We utilized MNI-137, a $mGlu_{2/3}$ NAM, as a positive control in our GIRK assay,[61] and found no evidence of $mGlu_3$ potencies up to the highest concentration of 30 μM. In addition, QCA was inactive towards other mGlu receptors at the test concentration of 30 μM, and showed no significant interaction with major CNS targets, which was conducted via GPCRome assays[62] developed by the NIH PDSP program. (see excel data sheet in the associate content).

We next evaluated whether QCA inhibits $mGlu_2$ by a competitive or noncompetitive mechanism of action in functional studies by performing a Schild analysis.[63] For these studies, the concentration-response relationships of glutamate-induced increases in thallium flux were evaluated for both $mGlu_2$ and $mGlu_3$ in the absence or presence (30 μM, 10 μM, 3333 nM, 1111 nM, 370 nM, 123 nM, or 41 nM) of QCA (Figure 3). QCA dose-dependently right-shifted the concentration-response of glutamate toward $mGlu_2$ (Figure 3A) and decreased the maximal glutamate response, consistent with a noncompetitive mode of action. Alternatively, consistent with the previous in vitro studies (Figure 2B), QCA had no effect on either the glutamate potency or glutamate maximal response toward $mGlu_3$ (Figure 3B), which also serves as an additional control demonstrating the $mGlu_2$ selectivity of QCA.

Lipophilicity of candidate compounds can be used as a predictive parameter for assessing blood-brain barrier permeability, with preferred range of 1.0–3.5.[64–66] The cLog*P* values of compounds QCA (**16**), FEQCA (**18**) and FPQCA (**19**) were predicted to be 2.95, 3.44 and 3.69, respectively, using Pallas 3.0 prediction software (Table 1). Using liquid-liquid partition between *n*-octanol and water ("shake flask method"),[67] the Log*P* values for QCA, FEQCA, and FPQCA were 1.27 ± 0.29, 1.75 ± 0.14 and 1.99 ± 0.12, respectively. Since *in vitro* assessments of pH stability, plasma and microsomal stability are important to the initial selection of candidate compounds,[68] we carried out preliminary experiments to determine these parameters. We first evaluated the stability of the compounds under physiological conditions (pH = 5.0–9.4). All three compounds showed excellent stability at pH 5 and diminished stability at pH 7.4 and 9.4 at 37°C, which may be attributed to hydrolysis of succinimidyl group at higher pH. In addition, QCA and its fluorinated derivatives showed reasonable plasma and microsomal stability. Based on the functional assay results (*cf.* Figs. 2 & 3) and physicochemical properties (*cf.* Table 1), QCA (**16**) exhibited the lowest EC_{50} value among all derivatives and reasonable lipophilicity and plasma/microsomal stability, which warrants further radiolabeling and subsequent evaluation by in vivo PET imaging and ex vivo biodistribution studies.

Radiochemistry

As shown in Scheme 2, there are three possible labeling strategies for QCA (**16**), namely (1) ^{11}C-cyanation followed by H_2O_2 hydrolysis from 2-chloroquinoline precursor; (2) ^{11}C-carbonylation via [^{11}C]CO followed by aminolysis from 2-chloroquinoline precursor and (3) ^{11}C-methylation from the the phenolic precursor **17**. Although the first two approaches may entail a general and unified strategy for the formation of ^{11}C-carbonyl labeled quinoline carboxamides, as proof of concept, we chose the most convenient phenolic site for QCA labeling. The radiosynthesis of [^{11}C]QCA was performed by the reaction of the phenolic precursor **17** (0.5 mg) with [^{11}C]CH_3I in the presence of NaOH (1.25 μmol) in DMF (300 μL). The reaction was carried out at 80 °C for 5 min, followed by purification using semi-preparative HPLC. Specifically, [^{11}C]QCA was obtained from the reaction between its phenolic precursor and [^{11}C]CH_3I. The radiochemical yield was 13 ± 4% non-decay corrected (n = 3), calculated from starting [^{11}C]CO_2. The [^{11}C]QCA was then reformulated in a saline solution containing 100 μL of 25% ascorbic acid in sterile water and 100 μL of 20% Tween® 80 in ethanol at the end of synthesis (see details in Methods). The radiochemical and chemical purity were greater than 99% and specific activity was greater than 74 GBq/μmol (2 Ci/μmol). The overall synthesis time was *ca.* 30 min and no radiolysis was observed up to 90 min.

Whole body biodistribution studies in mice

The uptake, distribution and clearance of [^{11}C]QCA ([^{11}C]**16**) were studied in mice at five time points (1, 5, 15, 30 and 60 min) post tracer injection. The results are expressed as the percentage of the injected dose per gram of wet tissue (%ID/g) in Figure 4 and Table S1 (SI) and standardized uptake value (SUV) in Figure S1 and Table S2 (SI). High uptake (>3% ID/g) was observed in the heart, lungs, liver, pancreas, kidneys and small intestine at 1 min post injection of [^{11}C]QCA. After the initial phase the radioactivity levels in most tissues decreased rapidly, while the signals in the liver and small intestine continually increased

until 30 min and then decreased slowly. The radioactivity was efficiently cleared from blood (1 min/60 min ratio of 2.4) and high radioactivity in the liver, kidneys and small intestine indicated urinary and hepatobiliary excretion, as well as a possible intestinal reuptake pathway. The distribution of [^{11}C]QCA in the peripheral organs was similar to prior reports with other compounds,[51,56,69,70] in which rapid clearance of radioactivity from heart, lungs, spleen and muscle was observed. Limited brain uptake (peak value 0.42% ID/g at 1 min post injection) was observed, and thus the regional brain distribution was further studied by in vitro autoradiography.

In vitro Autoradiography

The binding specificity of [^{11}C]QCA to $mGlu_2$ was confirmed by in vitro autoradiography. Representative in vitro autograms of [^{11}C]QCA on sagittal sections of rat brains are shown in Figure 5A. In the baseline study, the distribution of bound radioactivity was heterogeneous with signal levels from high to low in the order of cerebral cortex, striatum, hippocampus, cerebellum and pons/medulla (Figure 5B). These autographic results are in agreement with both the previously published distribution of $mGlu_2$ in rat brain,[10,12] and with other autoradiography studies with the $mGlu_2$ radioligands [^{11}C]CMDC,[51] [^{3}H]JNJ-40068782,[54] [^{3}H]LY341495[71] and [^{3}H]LY459477.[14] As shown in Figure 5C, quantitative analysis of radioactivity binding in the $mGlu_2$-rich regions (cerebral cortex, striatum, hippocampus and cerebellum) with unlabeled QCA (1 μM) and a NAM MNI-137[61] (1 μM) showed ca. 50–60% reduced binding compared with that of baseline. We also observed marginal reductions (ca. 10–20%) of radioactivity binding when a $mGlu_2$ PAM LY487379[72] was used for blocking study, which may indicate a possible shared, yet at a low level, binding site between positive and negative allosteric modulators.[73,74] These results indicate that [^{11}C]QCA has a moderate-to-high level of in vitro specific binding to $mGlu_2$ and the binding mechanism is consistent with that of a negative allosteric modulator.

PET imaging studies in normal rat brain

Dynamic PET acquisitions were carried out with [^{11}C]QCA in Sprague-Dawley rats for 60 min. Representative PET images (summed 0–60 min) in whole brain and time-activity curves are shown in Figure 6. The tracer [^{11}C]QCA showed limited brain uptake (*ca.* 0.3 SUV whole brain) in rat and no obvious washout (ratio of $SUV_{5\ min}/SUV_{90\ min}$ = 1.1). Pretreatment with unlabeled QCA (1 mg/kg) failed to show significant reduction of brain uptake, likely attributed to low brain permeability and possible *in vivo* non-specific binding (Figure 6C). We next carried out radiometabolite analysis and PET imaging in PgP/Bcrp knockout mice to investigate possible reasons of limited CNS penetration.

Radiometabolite analysis

To evaluate the in vivo stability of [^{11}C]QCA, radiometabolites in the plasma and brain homogenate of Sprague-Dawley rats were evaluated post-tracer injection. The percentages of unchanged [^{11}C]QCA and the corresponding radiometabolites, as determined by radio-HPLC, are shown in Figure 7. The fraction corresponding to unchanged [^{11}C]QCA in plasma was 93% at 5 min, 88% at 20 min and 79% at 60 min, respectively, with only one other more polar metabolite observed (Top three possible sites for the metabolism are predicted by SMARTCyp[75] and the results are listed as Table S3 in the supporting

information). Analysis of rat brain homogenates in the same time interval showed unchanged [^{11}C]QCA was 78%, 41% and 34%, respectively, with the same radiometabolite as found in plasma. These results indicate that the resulting polar radiometabolite may be brain penetrant.

PET imaging studies in PgP/Bcrp knockout mice

Based on the results of in vitro autoradiography and in vivo PET studies on rat brain, we speculated that insufficient brain permeability of [^{11}C]QCA might be induced by ATP-binding cassette efflux transporters located at the blood-brain barrier,[66,76–79] particularly, P-glycoprotein (PgP, ABCB1) and breast cancer resistance protein (Bcrp, ABCG2). To test this hypothesis, we carried out PET imaging studies of [^{11}C]QCA on wild-type and PgP/Bcrp knockout (ABCB1a/1b$^{-/-}$ABCG2$^{-/-}$) mice, and compared pharmacokinetic profiles, particularly brain uptake and clearance.

As shown in Figure 8, peak brain uptake in whole brain was *ca.* 0.8 SUV in PgP/Bcrp knockout mice, indicating a significant difference compared with that (*ca.* 0.3 SUV) of the wild-type mice. Whole brain uptake increased 130% in PgP/Bcrp knockout mice compared with that of wild-type mice (calculated based on area under curve). Therefore these results indicated that [^{11}C]QCA had intensive interactions with brain efflux pumps on the murine blood-brain barrier and is likely a PgP/Bcrp substrate in rodents.

CONCLUSION

We have efficiently synthesized a focused library of NAMs targeting $mGlu_2$, and radiolabeled the most promising ligand, namely [^{11}C]QCA in good radiochemical yield, high radiochemical purity and high specific activity. The pharmacokinetic profile (ex vivo distribution, uptake and clearance), in vitro autoradiography, brain penetration, efflux pump and metabolism studies were evaluated to determine the suitability of [^{11}C]QCA as a $mGlu_2$ tracer. While [^{11}C]QCA is not likely pursued for in vivo mapping of $mGlu_2$ due to limited brain permeability, in vitro specific binding studies by autoradiography showed promise as a new chemotype for $mGlu_2$ tracer development. Further SAR studies of succinimidyl and/or quinoline carboxamide functionality are necessary to test PgP/Bcrp efflux liability and to facilitate next generation tracer design with improved brain permeability. In-depth pharmacology evaluation is equally important to validate *in vivo* specificity using $mGlu_2$ knockout mice and/or $mGlu_2$-specific NAMs. Radiotracer's binding will also be evaluated under different agonist concentrations to characterize and select NAM- or PAM-based tracer for future clinical translation."

METHODS

Materials and Methods

General Consideration—All the chemicals employed in the syntheses were purchased from commercial vendors and used without further purification. Thin-layer chromatography (TLC) was conducted with 0.25 mm silica gel plates ($^{60}F_{254}$) and visualized by exposure to UV light (254 nm) or stained with potassium permanganate. Flash column chromatography was performed using silica gel (particle size 0.040–0.063 mm). H-Nuclear magnetic

resonance (NMR) spectra were obtained on a 300 MHz on Bruker spectrometers and ^{13}C NMR spectra were obtained at 75 MHz. Chemical shifts (δ) are reported in ppm and coupling constants are reported in Hertz. The multiplicities are abbreviated as follows: s = singlet, d = doublet, t = triplet, q = quartet, quint = quintet, sext = sextet, sept = setpet, m = multiplet, br = broad signal, dd = doublet of doublets. For LC-MS/MS measurements, the ionization method is ESI using Agilent 6430 Triple Quad LC/MS. Lipophilicity was calculated by Pallas 3.4 ADME prediction software (CompDrug International, Inc., USA). The animal experiments were approved by the Institutional Animal Care and Use Committee of Massachusetts General Hospital or the Animal Ethics Committee at the National Institute of Radiological Sciences. DdY mice (male; 7 weeks, 34–36 g), Pgp/Bcrp knockout (Abcb1a/1b$^{-/-}$Abcg2$^{-/-}$; male; 17–18 weeks old; 31–33 g), wild-type (male; 17–18 weeks old; 30–32 g) FAB mice and Sprague-Dawley rats (male; 7 weeks; 210–230 g) were kept on a 12 h light/12 h dark cycle and were allowed food and water *ad libitum*.

Chemistry

7-methylquinoline-2-carbonitrile (8)—7-methylquinoline (10 g, 57.9 mmol) was dissolved in dichloromethane (200 mL) in a round bottom flask with a stir bar. 3-Chloroperoxybenzoic acid (14.4 g, 75%, 75.33 mmol) was added in portions with ice bath. The mixture was stirred at room temperature overnight, then quenched with 400 mL 1N $NaOH_{(aq.)}$ and extracted with dichloromethane (200 mL × 3). The combined organic layers were washed with saturated aqueous sodium bicarbonate, dried over $MgSO_4$ and concentrated to give 7-methylquineline *N*-oxide. The crude product was used without further purification. To a solution of 7-methylquinoline *N*-oxide in dichloromethane (200 mL) was added trimethylsilyl cyanide (11.9g, 120.6 mmol) and dimethylcarbamoyl chloride (13.0 g 120.6 mmol). The mixture was stirred at room temperature overnight, then quenched with saturated sodium bicarbonate and extracted with dichloromethane (200 mL × 3). The combined organic layers were washed with saturated aqueous sodium chloride, dried over $MgSO_4$ and concentrated *in vacuo*. The residue was purified by flash chromatography on silica gel (hexanes to ethyl acetate gradient column) to yield the compound **8** as white solid (7.3 g, 74% over two steps). R_f = 0.3 (Hexanes/EtOAc = 20:1). ^1H NMR (400 MHz, $CDCl_3$) δ 8.27 (d, J = 8.3 Hz, 1H), 7.95 (s, 1H), 7.81 (d, J = 8.4 Hz, 1H), 7.66 (d, J = 8.3 Hz, 1H), 7.58 – 7.52 (m, 1H), 2.62 (s, 3H). ^{13}C NMR (100 MHz, $CDCl_3$) δ 148.3, 142.1, 137.1, 133.3, 131.8, 128.6, 127.3, 126.8, 122.6, 117.5, 21.9.

4-chloro-7-methylquinoline-2-carbonitrile (9)—Compound **8** (7.0 g, 41.6 mmol) was dissolved in dichloromethane (300 mL) in a round bottom flask with a stir bar. 3-Chloroperoxybenzoic acid (28.7 g, 75%, 124.8 mmol) was added in portions with ice bath. The mixture was stirred at 40°C for 3 h, then additional 3-chloroperoxybenzoic acid (28.7 g, 75%, 124.8 mmol) was added. The mixture was stirred at room temperature overnight, then quenched with 400 mL 1N $NaOH_{(aq.)}$ and extracted with dichloromethane (200 mL × 3). The combined organic layers were washed with saturated aqueous sodium bicarbonate, dried over $MgSO_4$ and concentrated to give 4-chloro-7-methylquinoline-2-carbonitrile *N*-oxide. The crude product was used without further purification. To a solution of 4-chloro-7-methylquinoline-2-carbonitrile *N*-oxide in chloroform (200 mL) was added DMF (3.0 g, 41.3 mmol). Then $POCl_3$ (38.0 g, 247.6 mmol) was added in three portions at 70°C in 4 h.

The mixture was stirred at 70 °C for 2 h before pour into iced water and extracted with dichloromethane (200 mL × 3). The combined organic layers were washed with saturated aqueous sodium chloride, dried over $MgSO_4$ and concentrated *in vacuo*. The residue was purified by flash chromatography on silica gel (hexanes to ethyl acetate gradient column) to yield the compound **9** as white solid (5.4 g, 64% over two steps). R_f = 0.3 (Hexanes/EtOAc = 20:1). ^{1}H NMR (400 MHz, $CDCl_3$) δ 8.17 (d, J = 8.6 Hz, 1H), 8.00 – 7.91 (m, 1H), 7.72 (s, 1H), 7.64 (dd, J = 8.7, 1.7 Hz, 1H), 2.62 (s, 3H). ^{13}C NMR (100 MHz, $CDCl_3$) δ 149.0, 143.7, 143.0, 133.1, 132.8, 129.2, 125.3, 123.8, 122.5, 116.7, 21.8.

7-(bromomethyl)-4-chloroquinoline-2-carbonitrile (10)—To a solution of the compound **9** (1.17 g, 5.76 mmol) in CCl_4 (110 mL) under Ar was added *N*-bromosuccinimide (1.13 g, 6.33 mmol) and benzoyl peroxide (139.50 mg, 0.579 mmol). The mixture was stirred at 85°C for 4 h, then quenched with water (50 mL) and extracted with dichloromethane (100 mL × 3). The combined organic layers were washed with saturated aqueous sodium chloride, dried over $MgSO_4$ and concentrated *in vacuo*. The residue was purified by flash chromatography on silica gel (hexanes to ethyl acetate gradient column) to yield the compound **10** as white solid (60%, 967 mg). R_f = 0.2 (Hexanes/EtOAc = 20:1). ^{1}H NMR (400 MHz, $CDCl_3$) δ 8.29 (d, J = 8.6 Hz, 1H), 8.17 (s, 1H), 7.84 (d, J = 8.6 Hz, 1H), 7.80 (s, 1H), 4.68 (s, 2H). ^{13}C NMR (100 MHz, $CDCl_3$) δ 148.7, 144.0, 142.1, 133.8, 131.4, 129.8, 126.8, 125.1, 123.7, 116.4, 31.5.

4-chloro-7-((2,5-dioxopyrrolidin-1-yl)methyl)quinoline-2-carbonitrile (11)—To a solution of the compound **10** (719 mg, 2.55 mmol) and succinimide (303 mg, 3.06 mmol) in DMF (15 mL) was added Cs_2CO_3 (1.66 g, 5.11 mmol). The mixture was stirred at room temperature for 0.5 h, then quenched with saturated aqueous KH_2PO_4 (40 mL) and extracted with ethyl acetate (40 mL × 3). The combined organic layers were washed with saturated aqueous sodium chloride, dried over $MgSO_4$ and concentrated *in vacuo*. The residue was purified by flash chromatography on silica gel (hexanes to ethyl acetate gradient column) to yield the compound **11** as white solid (80%, 612 mg). R_f = 0.2 (Hexanes/EtOAc = 1:1). ^{1}H NMR (400 MHz, $CDCl_3$) δ 8.25 (d, J = 8.7 Hz, 1H), 8.09 (s, 1H), 7.80 (d, J = 8.8 Hz, 1H), 7.77 (s, 1H), 4.92 (s, 2H), 2.81 (s, 4H). ^{13}C NMR (100 MHz, $CDCl_3$) δ 176.5, 148.7, 144.0, 140.0, 133.6, 130.9, 129.3, 126.6, 124.8, 123.4, 116.4, 41.8, 28.2.

7-((2,5-dioxopyrrolidin-1-yl)methyl)-4-(2-fluoro-4-methoxyphenyl)quinoline-2-carboxamide (QCA; 16)—To a solution of the 2-fluoro-4-methoxyphenylboronic acid (54.4 mg, 0.320 mmol) and Na_2CO_3 (56.6 mg, 0.534 mmol) in 1,4-dioxane : water (v/v, 10/1, 1.8 mL) was added compound **11** (80.0 mg, 0.267 mmol) and $Pd(PPh_3)_4$ (30.9 mg, 0.0267 mmol) under Ar. The mixture was stirred at 100°C for 4 h, then quenched with water (3 mL) and extracted with ethyl acetate (5 mL × 3). The combined organic layers were washed with saturated aqueous sodium chloride, dried over $MgSO_4$ and concentrated *in vacuo*. The residue was used without further purification. To the residue solution in acetone : water (v/v, 2/1, 15 mL) was added sodium percarbonate (0.251 g, 1.60 mmol). The mixture was stirred at room temperature for 4h, then added ethyl acetate (5 mL) and extracted with ethyl acetate (5 mL × 3). The residue was purified by flash chromatography on silica gel (hexanes to ethyl acetate gradient column) to yield QCA (**16**) as white solid (42% for two

steps, 55 mg). R_f = 0.2 (Hexanes/EtOAc = 1:3). ^{1}H NMR (300 MHz, DMSO-d_6) δ 8.02 (s, 1H), 8.01 (s, 1H), 7.97 (s, 1H), 7.82 (s, 1H), 7.69 – 7.56 (m, 2H), 7.46 (t, J = 8.6 Hz, 1H), 6.86 – 6.72 (m, 2H), 4.78 (s, 2H), 3.87 (s, 3H), 2.73 (s, 4H). ^{13}C NMR (75 MHz, DMSO-d_6) δ 178.1, 166.4, 161.9 (d, J = 11.0 Hz), 160.0 (d, J = 244.1 Hz), 150.8, 146.8, 143.7, 139.2, 132.6 (d, J = 4.9 Hz), 128.9, 128.3, 126.8, 126.3, 120.0, 116.7 (d, J = 15.9 Hz), 111.6, 102.4 (d, J = 25.4 Hz), 56.3, 41.6, 28.7.

7-((2,5-dioxopyrrolidin-1-yl)methyl)-4-(2-fluoro-4-hydroxyphenyl)quinoline-2-carboxamide (17)—To a solution of the 2-fluoro-4-hydroxyphenylboronic acid (50 mg, 0.320 mmol) and Na_2CO_3 (56.6 mg, 0.534 mmol) in 1,4-dioxane : water (v/v, 10/1, 1.8 mL) was added compound **11** (80.0 mg, 0.267 mmol) and $Pd(PPh_3)_4$ (30.9 mg, 0.0267 mmol) under Ar. The mixture was stirred at 100°C for 4 h, then quenched with water (3 mL) and extracted with ethyl acetate (5 mL × 3). The combined organic layers were washed with saturated aqueous sodium chloride, dried over $MgSO_4$ and concentrated *in vacuo*. The residue was used without further purification. To the residue solution in acetone : water (v/v, 2/1, 1.5 mL) was added sodium percarbonate (0.251 g, 1.60 mmol). The mixture was stirred at room temperature for 4 h, then added ethyl acetate (5mL) and extracted with ethyl acetate (5 mL × 3). The residue was purified by flash chromatography on silica gel (hexanes to ethyl acetate gradient column) to yield the compound **13** as white solid (39% for two steps, 49 mg). R_f = 0.2 (Hexanes/EtOAc = 1:3). ^{1}H NMR (300 MHz, DMSO-d_6) δ 10.32 (s, 1H), 8.31 (s, 1H), 8.01 (s, 1H), 7.96 (s, 1H), 7.81 (s, 1H), 7.71 – 7.66 (m, 2H), 7.34 (t, J = 8.6 Hz, 1H), 6.86 – 6.72 (m, 2H), 4.78 (s, 2H), 2.73 (s, 4H). ^{13}C NMR (75 MHz, DMSO-d_6) δ 177.6, 166.0, 159.6 (d, J = 243.7 Hz), 160.0 (d, J = 11.7 Hz), 150.3, 146.4, 143.6, 138.6, 132.2 (d, J = 5.0 Hz), 128.4, 127.9, 126.5, 126.0, 119.5, 114.7 (d, J = 15.7 Hz), 112.3, 103.0 (d, J = 24.1 Hz), 41.2, 28.2.

7-((2,5-dioxopyrrolidin-1-yl)methyl)-4-(2-fluoro-4-(2-fluoroethoxy)phenyl)quinoline-2-carboxamide (FEQCA; 18)—To a solution of the 2-fluoro-4-hydroxyphenylboronic acid (50 mg, 0.320 mmol) and Na_2CO_3 (56.6 mg, 0.534 mmol) in 1,4-dioxane : water (v/v, 10/1, 1.8 mL) was added compound **11** (80.0 mg, 0.267 mmol) and $Pd(PPh_3)_4$ (30.9 mg, 0.0267 mmol) under Ar. The mixture was stirred at 100°C for 4 h, then quenched with water (3 mL) and extracted with ethyl acetate (5 mL × 3). The combined organic layers were washed with saturated aqueous sodium chloride, dried over $MgSO_4$ and concentrated *in vacuo*. The residue was used without further purification. To the residue solution in DMF (1.5 mL) was added 1-fluoro-2-iodoethane (112 mg, 0.640 mmol) and Cs_2CO_3 (209 mg, 0.640 mmol). The mixture was stirred at room temperature overnight, then quenched with saturated aqueous KH_2PO_4 (5 mL). The combined organic layers were washed with saturated aqueous sodium chloride, dried over $MgSO_4$ and concentrated *in vacuo*. The residue was purified by flash chromatography on silica gel (hexanes to ethyl acetate gradient column) to yield the compound **14** as white solid (45% for two steps, 50.6 mg) and used directly in the next step. To the solution of compound **14** (42.1 mg, 0.1 mmol) in acetone : water (v/v, 2/1, 2 mL) was added sodium percarbonate (78 mg, 0.50 mmol). The mixture was stirred at room temperature for 4h, then added ethyl acetate (5 mL) and extracted with ethyl acetate (5 mL × 3). The residue was purified by flash chromatography on silica gel (hexanes to ethyl acetate gradient column) to yield FEQCA (**18**) as white solid

(60%, 26.3 mg). R_f = 0.2 (Hexanes/EtOAc = 1:3). ^{1}H NMR (300 MHz, DMSO-d_6) δ 8.34 (s, 1H), 8.03 (s, 1H), 7.99 (s, 1H), 7.83 (s, 1H), 7.69 – 7.59 (m, 2H), 7.47 (t, J = 8.6 Hz, 1H), 7.45 – 7.02 (m, 2H), 4.79 (dt, J=47.9, 3.5 Hz), 4.78 (s, 2H), 4.37 (dt, J=30.0, 3.5 Hz), 2.73 (s, 4H). ^{13}C NMR (75 MHz, DMSO-d_6) δ 178.1, 166.4, 160.0 (d, J = 243.8 Hz), 160.6 (d, J = 11.1 Hz), 150.7, 146.8, 143.6, 139.2, 134.7 (d, J = 4.7 Hz), 128.9, 128.4, 126.7, 126.3, 120.0, 117.1 (d, J = 15.8 Hz), 112.0, 103.0 (d, J = 25.7 Hz), 82.4 (d, J = 165.6 Hz), 68.2 (d, J = 18.8 Hz), 41.6, 28.6.

7-((2,5-dioxopyrrolidin-1-yl)methyl)-4-(2-fluoro-4-(3-fluoropropoxy)phenyl)quinoline-2-carboxamide (FPQCA; 19)—To a solution of the 2-fluoro-4-hydroxyphenylboronic acid (50 mg, 0.320 mmol) and Na_2CO_3 (56.6 mg, 0.534 mmol) in 1,4-dioxane : water (v/v, 10/1, 1.8 mL) was added compound **11** (80.0 mg, 0.267 mmol) and $Pd(PPh_3)_4$ (30.9 mg, 0.0267 mmol) under Ar. The mixture was stirred at 100°C for 4 h, then quenched with water (3 mL) and extracted with ethyl acetate (5 mL × 3). The combined organic layers were washed with saturated aqueous sodium chloride, dried over $MgSO_4$ and concentrated *in vacuo*. The residue was used without further purification. To the residue solution in DMF (1.5 mL) was added 1-fluoro-3-iodopropane (120 mg, 0.640 mmol) and Cs_2CO_3 (209 mg, 0.640 mmol). The mixture was stirred at room temperature overnight, then quenched with saturated aqueous KH_2PO_4 (5 mL). The combined organic layers were washed with saturated aqueous sodium chloride, dried over $MgSO_4$ and concentrated *in vacuo*. The residue was purified by flash chromatography on silica gel (hexanes to ethyl acetate gradient column) to yield the compound **15** as white solid (47% for two steps, 54.6 mg) and used directly in the next step. To the solution of compound **15** (43.6 mg, 0.1 mmol) in acetone : water (v/v, 2/1, 2 mL) was added sodium percarbonate (78 mg, 0.50 mmol). The mixture was stirred at room temperature for 4 h, then added ethyl acetate (5 mL) and extracted with ethyl acetate (5 mL × 3). The residue was purified by flash chromatography on silica gel (hexanes to ethyl acetate gradient column) to yield FPQCA (**19**) as white solid (53%, 24 mg). R_f = 0.2 (Hexanes/EtOAc = 1:3). ^{1}H NMR (300 MHz, DMSO-d_6) δ 8.33 (s, 1H), 8.02 (s, 1H), 7.97 (s, 1H), 7.82 (s, 1H), 7.69 – 7.57 (m, 2H), 7.46 (t, J=8.6 Hz, 1H), 7.45 – 7.02 (m, 2H), 4.78 (s, 2H), 4.63 (dt, J = 47.3, 5.9 Hz), 4.19 (t, J = 6.3 Hz), 2.73 (s, 4H), 2.22 – 2.07 (m, 2H). ^{13}C NMR (75 MHz, DMSO-d_6) δ 178.1, 166.4, 160.0(d, J = 244.4 Hz), 161.0 (d, J = 12.5 Hz), 150.7, 146.8, 143.7, 139.2, 132.6 (d, J = 5.0 Hz), 128.9, 128.3, 126.8, 126.3, 120.0, 116.8 (d, J = 16.0 Hz), 112.0, 102.9 (d, J = 25.6 Hz), 81.2 (d, J = 160.7 Hz), 64.7 (d, J = 5.3 Hz), 41.6, 64.7 (d, J = 19.6 Hz), 28.6.

Pharmacology

Cell line generation and thallium flux assays—In order to generate human $mGlu_2$ and $mGlu_3$ stable cell lines to be used for thallium flux assays, human $mGlu_2$ and $mGlu_3$ were prepared by PCR amplification of the entire coding sequence of each receptor and cloning into pIRES puro 3 (Invitrogen). For $mGlu_2$ and $mGlu_3$, the cloning sites were NheI/NotI. HEK GIRK cells, generously provided by Lily Jan (University of California San Francisco, San Francisco, CA), were transfected with 24 μg of DNA using Fugene6 (Promega), stable transfectants were selected with 1000 ng/mL puromycin dihydrochloride (Sigma-Aldrich, St. Louis, MO), and polyclonal human $mGlu_2$ GIRK and $mGlu_3$ GIRK cell lines were established. Cells were maintained following selection in 45% DMEM, 45%

Ham's F12, 10% FBS, 100 units/mL penicillin/streptomycin, 20 mM HEPES, pH 7.3, 1 mM sodium pyruvate, 2 mM glutamine, 700 μg/mL G418 (Mediatech, Inc., Herndon, VA), and 600 μg/mL puromycin (growth media) at 37°C in the presence of 5% CO_2. All cell culture reagents were purchased from Invitrogen Corp. (Carlsbad, CA) unless otherwise noted.

Human $mGlu_2$ and $mGlu_3$ thallium flux in vitro assays—Compound activity at $mGlu_2$ and $mGlu_3$ was assessed using thallium flux through GIRK channels, a method that has been described in detail.[80,81] Briefly, cells were plated into 384-well, black-walled, clear-bottomed poly-D-lysine-coated plates at a density of 15,000 cells/20 μL/well in DMEM containing 10% dialyzed FBS, 20 mM HEPES, and 100 units/mL penicillin/streptomycin (assay media). Plated cells were incubated overnight at 37°C in the presence of 5% CO_2. The following day, the medium was exchanged from the cells to assay buffer [Hanks' balanced salt solution (Invitrogen) containing 20 mM HEPES, pH 7.3] using an ELX405 microplate washer (BioTek), leaving 20 μL/well, followed by the addition of 20 μL/well FluoZin2-AM (330 nM final concentration) indicator dye (Invitrogen; prepared as a stock in DMSO and mixed in a 1:1 ratio with Pluronic acid F-127) in assay buffer. Cells were incubated for 1 h at room temperature, and the dye exchanged to assay buffer using an ELX405, leaving 20 μL/well. For concentration-response curve experiments, compounds were serially diluted 1:3 into 10 point concentration response curves and were transferred to daughter plates using an Echo acoustic plate reformatter (Labcyte, Sunnyvale, CA). Test compounds were diluted to 2 times their final desired concentration in assay buffer (0.3% DMSO final concentration). Agonists were diluted in thallium buffer [125 mM sodium bicarbonate (added fresh the morning of the experiment), 1 mM magnesium sulfate, 1.8 mM calcium sulfate, 5 mM glucose, 12 mM thallium sulfate, and 10 mM HEPES, pH 7.3] at 5 times the final concentration to be assayed. Cell plates and compound plates were loaded onto a kinetic imaging plate reader (FDSS 6000 or 7000; Hamamatsu Corporation, Bridgewater, NJ). Appropriate baseline readings were taken (10 images at 1 Hz; excitation, 470 ± 20 nm; emission, 540 ± 30 nm) and test compounds were added in a 20 μL volume and incubated for approximately 1 hour at room temperature before the addition of 10 μL of thallium buffer with or without an EC_{80} concentration of the agonist glutamate for potency evaluation experiments or with a full concentration-response of glutamate for Schild analysis experiments. After the addition of agonist, data were collected for approximately an additional 2.5 min. Data were analyzed using Excel (Microsoft Corp, Redmond, WA). The slope of the fluorescence increase beginning 5 s after thallium/agonist addition and ending 15 s after thallium/agonist addition was calculated, corrected to vehicle and maximal agonist control slope values, and plotted in using either XLfit (ID Business Solutions Ltd) or Prism software (GraphPad Software, San Diego, CA) to generate concentration-response curves. Potencies were calculated from fits using a four-point parameter logistic equation.

Measurement of physicochemical properties

Measurement of partition coefficient (LogP) ("shake flask method")—The measurement of Log*P* value was performed by mixing test compound (50μL, 20 μM in DMSO) with *n*-octanol (475 μL) and water (475 μL) in a test tube. The *n*-octanol and water were pre-saturated with each other before use. The tube was vortexed for 1 min before shaken at 37°C overnight. Water phase and *n*-octanol phase (200 μL each) were aliquoted.

The amount of the test compound in each phase was determined by LC-MS/MS (Agilent 6430 Triple Quad LC/MS). The Log*P* was calculated by Log [ratio between the amount of test compound in *n*-octanol and water solution]. The procedure was repeated triplicate and the value was shown in Table 1.

Measurement of pH stability—The stability of compounds in buffer solutions was measured using a HPLC method adapted from our previous protocol.[82] Briefly, testing compounds **16**, **18**–**19** (0.25 μmol) were each dissolved in 1 mL DMSO to make a stock solution. An aliquot (50 μL stock solution) was mixed with phosphate buffer (950 μL, 20 mM, pH 7.4), boric acid-KCl-NaOH buffer (950 μL, 20 mM, pH 9.4) or sodium acetate-KCl-HCl buffer (950 μL, 20 mM, pH 5.0) and incubated for 1 h at 37 °C. The percentage of the unchanged compound was monitored by HPLC (Luna analytical column, 4.6 × 250 mm, 5 μm, CH_3CN/H_2O + 0.1% TFA).

Measurement of plasma stability—The stability of candidate compounds in rat serum was measured using a literature method.[83] Briefly, the test was performed by mixing a candidate compound (10 μL, 10 μM in DMSO stock solution) with 250 μL aliquot of rat serum (Abcam, Inc. No. ab7488) in a test tube. The tube was vortexed before incubated at 37°C for 60 min. The reaction was quenched by the addition of 250 μL ice-cold CH_3CN, followed by centrifuge at 10,000 × g for 10 min. The amount of the test compound was quantified by LC-MS/MS (Agilent 6430 Triple Quad LC/MS). The percentage remaining was calculated by (peak area at 60 min) / (peak area at 0 min)×100%. The procedure was repeated at least triplicate and diltiazem was used as a positive control.

Measurement of liver microsomal stability—The stability of candidate compounds in liver microsomes was measured using a literature method.[84] Briefly, the test was performed by mixing a candidate compound (0.5 μL, 2 mM in DMSO stock solution) with PBS (432 μL) and 13 μL aliquot of Sprague-Dawley rat liver microsomes (Sigma-Aldrich, No. M9066) in a test tube. The tube was vortexed before shaken at 37°C for 5 min, followed by the addition of NADPH (50 μL, 10 mM in PBS stock solution). The mixture was incubated at 37°C for 60 min, and quenched by the addition of 250μL ice-cold CH_3CN and centrifuge at 10,000 × g for 10 min. The amount of the test compound was quantified by LC-MS/MS (Agilent 6430 Triple Quad LC/MS). The percentage remaining was calculated by (peak area at 60 min)/(peak area at 0 min) × 100%. The procedure was repeated at least triplicate and verapamil was used as a positive control.

Radiochemistry

Radiolabeling of [^{11}C]QCA—[^{11}C]Methyl iodide ([^{11}C]CH_3I) was synthesized from cyclotron-produced [^{11}C]CO_2, which was produced by $^{14}N(p, \alpha)^{11}C$ nuclear reaction. Briefly, [^{11}C]CO_2 was bubbled into a solution of $LiAlH_4$ (0.4 M in THF, 300 μL). After evaporation, the remaining reaction mixture was treated with hydroiodic acid (57% aqueous solution, 300 μL). The resulting [^{11}C]CH_3I was transferred under helium gas with heating into a pre-cooled (−15 to −20 °C) reaction vessel containing precursor 17 (0.5 mg), NaOH (2.5 μL, 0.5 M) and anhydrous DMF (300 μL). After the radioactivity reached a plateau during transfer, the reaction vessel was warmed to 80 °C and maintained for 5 min.

CH_3CN/H_2O + 0.1% Et_3N (v/v, 4/6, 0.5 mL) was added to the reaction mixture, which was then injected to a semi-preparative HPLC system. HPLC purification was completed on a Capcell Pak UG80 C18 column (10 mm ID × 250 mm) using a mobile phase of CH_3CN/H_2O + 0.1% Et_3N (v/v, 4/6) at a flowrate of 6.0 mL/min. The retention time for [^{11}C]QCA was 9.5 min. The radioactive fraction corresponding to the desired product was collected in a sterile flask, evaporated to dryness *in vacuo*, and reformulated in a saline solution (3 mL) containing 100 μL of 25% ascorbic acid in sterile water and 100 μL of 20% Tween® 80 in ethanol. (Note: We added ascorbic acid to prevent potential radiolysis and Tween® 80 to improve aqueous solubility.) The synthesis time was *ca*. 30 min from end-of-bombardment. Radiochemical and chemical purity were measured by analytical HPLC (Capcell Pak UG80 C18, 4.6 mm ID × 250 mm, UV at 254 nm; CH_3CN / H_2O + 0.1% Et_3N (v/v, 4/6) at a flowrate of 1.2 mL/min). The identity of [^{11}C]QCA was confirmed by the co-injection with unlabeled QCA. Radiochemical yield was 46% decay-corrected based on [^{11}C]CO_2 with >99% radiochemical purity and greater than 2 Ci/μmol specific activity.

Ex vivo biodistribution in mice

A solution of [^{11}C]QCA (50 μCi/150–200 μL) was injected into DdY mice via the tail vein. These mice (n = 5, each time point) were sacrificed at 1, 5, 15, 30 and 60 min post tracer injection. Major organs, including whole brain, heart, liver, lung, spleen, kidneys, small intestine (including contents), muscle, testes, and blood samples were quickly harvested and weighted. The radioactivity present in these tissues was measured using a gamma counter (PerkinElmer, USA), and all radioactivity measurements were automatically decay corrected based on half-life of ^{11}C. The results are expressed as the percentage of injected dose per gram of wet tissue (% ID/g) or standardized uptake value (SUV).

In vitro autoradiography

Rat brain was cut into 20 μM sections and stored at −80°C until they were used for experiment. The rat brain sections were pre-incubated with Tris-HCl buffer (50 mM), $MgCl_2$ (1.2 mM) and $CaCl_2$ (2 mM) solution for 20 min at ambient temperature, followed by incubation with [^{11}C]QCA (0.48 nM). For blocking studies, unlabeled QCA (1 μM) was added to incubation solution in advance to determine the specificity of radioligand binding. After incubation, brain sections were rinsed with ice-cold buffer three times for 2 min, dipped in cold distilled water for 10 sec. The brain sections were dried with cold air, then placed on imaging plates (BAS-MS2025, GE Healthcare, NJ, USA) for optimized contact periods. Autoradiograms were obtained and ROIs were carefully drawn with the reference of naked-eye observation. Radioactivity was expressed as photostimulated luminescene values per unit area (PSL/mm^2) and measured by a Bio-Imaging analyzer system (BAS5000, Fujifilm)

Small-animal PET imaging studies

PET scans were acquired by an Inveon PET scanner (Siemens Medical Solutions, Knoxville, TN, USA). Sprague-Dawley rats were kept under anesthesia with 1–2% (v/v) isoflurane during the scan. The radiotracer (ca. 1 mCi/150–200 μL) was injected via a preinstalled catheter via tail vein. A dynamic scan in 3D list mode was acquired for 60 min. For pretreatment studies, QCA (1 mg/kg) pre-dissolved in 300 μL saline containing 10% ethanol

and 5% Tween® 80 was injected at 30 min via the tail vein catheter before the injection of [^{11}C]QCA.

As we previously reported,[78,79] the PET dynamic images were reconstructed using ASIPro VW software (Analysis Tools and System Setup/Diagnostics Tool, Siemens Medical Solutions). Volumes of interest, including the whole brain, cerebral cortex, cerebellum, striatum, thalamus and pons were placed using ASIPro software. The radioactivity was decay-corrected and expressed as the standardized uptake value. SUV = (radioactivity per mL tissue/injected radioactivity) × body weight.

Radiometabolite analysis

Following the intravenous injection of [^{11}C]QCA, Sprague-Dawley rats were sacrificed at 5, 20 and 60 min (n = 3 each time point). Blood and whole brain samples were quickly removed and the blood samples were centrifuged at 15,000 × g for 2 min at 4 °C to separate the plasma. The supernatant (0.5 mL) was then collected in a test tube containing CH_3CN (0.5 mL) and the resulting mixture was vortexed for 15s and centrifuged at 15,000 × g for 2 min for deproteinization. The rat brain was homogenized in an ice-cooled CH_3CN/H_2O (1 mL, 1/1, v/v) solution. The homogenate was centrifuged at 150,000 rpm for 2 min at 4 °C and the supernatant was collected. The recovery of radioactivity into the supernatant was > 90% based on the total radioactivity in the brain homogenate.

An aliquot of the supernatant (100 μL) obtained from the plasma or brain homogenate was injected into the radio-HPLC system, and analyzed using a Capcell Pak UG80 C18 column (4.6 mm ID × 250 mm) in a mobile phase of CH_3CN / H_2O + 0.1% Et_3N (v/v, 45/55) at a flowrate of 1.0 mL/min. The retention time of [^{11}C]QCA is 7.8 min. The percentage of [^{11}C]QCA to total radioactivity (corrected for decay) on the HPLC charts was calculated as (peak area for [^{11}C]QCA/total peak area) × 100.

Supplementary Material

Refer to Web version on PubMed Central for supplementary material.

Acknowledgments

We would like to thank the staff at the radiochemistry program, Massachusetts General Hospital, MA, USA and National Institutes for Quantum and Radiological Science and Technology, National Institute of Radiological Sciences, Chiba, Japan for their support. We thank the National Institute of Mental Health's Psychoactive Drug Screening Program (NIMH PDSP) for the compound screening. The NIMH PDSP is directed by Bryan L. Roth MD, PhD at the University of North Carolina at Chapel Hill and Project Officer Jamie Driscoll at NIMH, Bethesda MD, USA. We also thank Drs. Thomas J. Brady and Lei Zhang for helpful discussion. X.Z. is supported by China Scholarship Council Fellowship (201606200041). N.D.P.C. is supported by a National Institute of Mental Health grant (R01-MH106865). S.H.L is a recipient of NIH career development award from the National Institute on Drug Abuse (DA038000).

References

1. Nakanishi S. Molecular diversity of glutamate receptors and implications for brain function. Science. 1992; 258:597–603. [PubMed: 1329206]
2. Kew JN, Kemp JA. Ionotropic and metabotropic glutamate receptor structure and pharmacology. Psychopharmacology. 2005; 179:4–29. [PubMed: 15731895]

3. Bowie D. Ionotropic glutamate receptors & CNS disorders. CNS Neurol Disord Drug Targets. 2008; 7:129–143. [PubMed: 18537642]
4. Traynelis SF, Wollmuth LP, McBain CJ, Menniti FS, Vance KM, Ogden KK, Hansen KB, Yuan H, Myers SJ, Dingledine R. Glutamate receptor ion channels: structure, regulation, and function. Pharmacol Rev. 2010; 62:405–496. [PubMed: 20716669]
5. Lau A, Tymianski M. Glutamate receptors, neurotoxicity and neurodegeneration. Pflugers Arch. 2010; 460:525–542. [PubMed: 20229265]
6. Niciu MJ, Kelmendi B, Sanacora G. Overview of glutamatergic neurotransmission in the nervous system. Pharmacol Biochem Behav. 2012; 100:656–664. [PubMed: 21889952]
7. Niswender CM, Conn PJ. Metabotropic glutamate receptors: physiology, pharmacology, and disease. Annu Rev Pharmacol Toxicol. 2010; 50:295–322. [PubMed: 20055706]
8. Testa CM, Friberg IK, Weiss SW, Standaert DG. Immunohistochemical localization of metabotropic glutamate receptors $mGluR_{1a}$ and $mGluR_{2/3}$ in the rat basal ganglia. J Comp Neurol. 1998; 390:5–19. [PubMed: 9456172]
9. Schoepp DD. Unveiling the functions of presynaptic metabotropic glutamate receptors in the central nervous system. J Pharmacol Exp Ther. 2001; 299:12–20. [PubMed: 11561058]
10. Ohishi H, Shigemoto R, Nakanishi S, Mizuno N. Distribution of the messenger RNA for a metabotropic glutamate receptor, $mGluR_2$ in the central nervous system of the rat. Neuroscience. 1993; 53:1009–1018. [PubMed: 8389425]
11. Ohishi H, Ogawa-Meguro R, Shigemoto R, Kaneko T, Nakanishi S, Mizuno N. Immunohistochemical localization of metabotropic glutamate receptors, mGluR2 and mGluR3, in rat cerebellar cortex. Neuron. 1994; 13:55–66. [PubMed: 8043281]
12. Ohishi H, Neki A, Mizuno N. Distribution of a metabotropic glutamate receptor, $mGluR_2$, in the central nervous system of the rat and mouse: an immunohistochemical study with a monoclonal antibody. Neurosci Res. 1998; 30:65–82. [PubMed: 9572581]
13. Richards G, Messer J, Malherbe P, Pink R, Brockhaus M, Stadler H, Wichmann J, Schaffhauser H, Mutel V. Distribution and abundance of metabotropic glutamate receptor subtype 2 in rat brain revealed by [^{3}H]LY354740 binding in vitro and quantitative radioautography: Correlation with the sites of synthesis, expression, and agonist stimulation of [^{35}S]GTPγs binding. J Comp Neurol. 2005; 487:15–27. [PubMed: 15861463]
14. Wright RA, Johnson BG, Zhang C, Salhoff C, Kingston AE, Calligaro DO, Monn JA, Schoepp DD, Marek GJ. CNS distribution of metabotropic glutamate 2 and 3 receptors: transgenic mice and [^{3}H]LY459477 autoradiography. Neuropharmacology. 2013; 66:89–98. [PubMed: 22313530]
15. Hovelso N, Sotty F, Montezinho LP, Pinheiro PS, Herrik KF, Mork A. Therapeutic potential of metabotropic glutamate receptor modulators. Curr Neuropharmacol. 2012; 10:12–48. [PubMed: 22942876]
16. Soto D, Altafaj X, Sindreu C, Bayes A. Glutamate receptor mutations in psychiatric and neurodevelopmental disorders. Commun Integr Biol. 2014; 7:6.
17. Golubeva AV, Moloney RD, O'Connor RM, Dinan TG, Cryan JF. Metabotropic Glutamate Receptors in Central Nervous System Diseases. Curr Drug Targets. 2016; 17:538–616. [PubMed: 25777273]
18. Muguruza C, Meana JJ, Callado LF. Group II Metabotropic Glutamate Receptors as Targets for Novel Antipsychotic Drugs. Front Pharmacol. 2016; 7
19. Ribeiro FM, Vieira LB, Pires RG, Olmo RP, Ferguson SS. Metabotropic glutamate receptors and neurodegenerative diseases. Pharmacol Res. 2017; 115:179–191. [PubMed: 27872019]
20. Vaidya A, Jain S, Jain AK, Agrawal A, Kashaw SK, Jain SK, Agrawal RK. Metabotropic glutamate receptors: a review on prospectives and therapeutic aspects. Mini Rev Med Chem. 2013; 13:1967–1981. [PubMed: 22530579]
21. Cleva RM, Olive MF. mGlu receptors and drug addiction. Wiley Interdiscip Rev Membr Transp Signal. 2012; 1:281–295. [PubMed: 22662312]
22. Pomierny-Chamiolo L, Rup K, Pomierny B, Niedzielska E, Kalivas PW, Filip M. Metabotropic glutamatergic receptors and their ligands in drug addiction. Pharmacol Ther. 2014; 142:281–305. [PubMed: 24362085]

23. Kalivas PW, Volkow ND. New medications for drug addiction hiding in glutamatergic neuroplasticity. Mol Psychiatry. 2011; 16:974–986. [PubMed: 21519339]
24. Chiechio S, Nicoletti F. Metabotropic glutamate receptors and the control of chronic pain. Curr Opin Pharmacol. 2012; 12:28–34. [PubMed: 22040745]
25. Campo B, Kalinichev M, Lambeng N, El Yacoubi M, Royer-Urios I, Schneider M, Legrand C, Parron D, Girard F, Bessif A, Poli S, Vaugeois JM, Le Poul E, Celanire S. Characterization of an $mGluR_{2/3}$ negative allosteric modulator in rodent models of depression. J Neurogenet. 2011; 25:152–166. [PubMed: 22091727]
26. Dwyer JM, Lepack AE, Duman RS. $mGluR_{2/3}$ blockade produces rapid and long-lasting reversal of anhedonia caused by chronic stress exposure. J Mol Psychiatry. 2013; 1:15. [PubMed: 25408908]
27. Conn PJ, Lindsley CW, Jones CK. Activation of metabotropic glutamate receptors as a novel approach for the treatment of schizophrenia. Trends Pharmacol Sci. 2009; 30:25–31. [PubMed: 19058862]
28. Dickerson JW, Conn PJ. Therapeutic potential of targeting metabotropic glutamate receptors for Parkinson's disease. Neurodegener Dis Manag. 2012; 2:221–232. [PubMed: 23526920]
29. Samadi P, Rajput A, Calon F, Grégoire L, Hornykiewicz O, Rajput AH, Di Paolo T. Metabotropic Glutamate Receptor II in the Brains of Parkinsonian Patients. J Neuropathol Exp Neurol. 2009; 68:374–382. [PubMed: 19287314]
30. Lee HG, Zhu X, O'Neill MJ, Webber K, Casadesus G, Marlatt M, Raina AK, Perry G, Smith MA. The role of metabotropic glutamate receptors in Alzheimer's disease. Acta Neurobiol Exp. 2004; 64:89–98.
31. Celanire S, Sebhat I, Wichmann J, Mayer S, Schann S, Gatti S. Novel metabotropic glutamate receptor 2/3 antagonists and their therapeutic applications: a patent review (2005 - present). Expert Opin Ther Pat. 2015; 25:69–90. [PubMed: 25435285]
32. Melancon BJ, Hopkins CR, Wood MR, Emmitte KA, Niswender CM, Christopoulos A, Conn PJ, Lindsley CW. Allosteric modulation of seven transmembrane spanning receptors: theory, practice, and opportunities for central nervous system drug discovery. J Med Chem. 2012; 55:1445–1464. [PubMed: 22148748]
33. Lindsley CW, Emmitte KA, Hopkins CR, Bridges TM, Gregory KJ, Niswender CM, Conn PJ. Practical Strategies and Concepts in GPCR Allosteric Modulator Discovery: Recent Advances with Metabotropic Glutamate Receptors. Chem Rev. 2016; 116:6707–6741. [PubMed: 26882314]
34. Trabanco AA, Cid JM. mGluR2 positive allosteric modulators: a patent review (2009 - present). Expert Opin Ther Pat. 2013; 23:629–647. [PubMed: 23452205]
35. Felts AS, Rodriguez AL, Smith KA, Engers JL, Morrison RD, Byers FW, Blobaum AL, Locuson CW, Chang S, Venable DF, Niswender CM, Daniels JS, Conn PJ, Lindsley CW, Emmitte KA. Design of 4-Oxo-1-aryl-1,4-dihydroquinoline-3-carboxamides as Selective Negative Allosteric Modulators of Metabotropic Glutamate Receptor Subtype 2. J Med Chem. 2015; 58:9027–9040. [PubMed: 26524606]
36. Fowler JS, Wolf AP. Working against Time: Rapid Radiotracer Synthesis and Imaging the Human Brain. Acc Chem Res. 1997; 30:181–188.
37. Phelps ME. Positron emission tomography provides molecular imaging of biological processes. Proc Natl Acad Sci. 2000; 97:9226–9233. [PubMed: 10922074]
38. Lee C-M, Farde L. Using positron emission tomography to facilitate CNS drug development. Trends Pharmacol Sci. 2006; 27:310–316. [PubMed: 16678917]
39. Willmann JK, van Bruggen N, Dinkelborg LM, Gambhir SS. Molecular imaging in drug development. Nature reviews. Drug discovery. 2008; 7:591–607. [PubMed: 18591980]
40. Sobrio F. Radiosynthesis of carbon-11 and fluorine-18 labelled radiotracers to image the ionotropic and metabotropic glutamate receptors. J Labelled Comp Radiopharm. 2013; 56:180–186. [PubMed: 24285324]
41. Fuchigami T, Nakayama M, Yoshida S. Development of PET and SPECT Probes for Glutamate Receptors. Scientific World J. 2015:19.
42. Mu, L., Ametamey, SM. Current Radioligands for the PET Imaging of Metabotropic Glutamate Receptors. In: Dierckx, RAJO.Otte, A.de Vries, EFJ.van Waarde, A., Luiten, PGM., editors. PET

and SPECT of Neurobiological Systems. Springer Berlin Heidelberg; Berlin, Heidelberg: 2014. p. 409-443.

43. Zhang, Z., Brownell, A-L. Imaging of Metabotropic Glutamate Receptors (mGluRs). In: Bright, PP., editor. Neuroimaging - Clinical Applications. 2012.
44. Li D, Shan H, Conti P, Li Z. PET imaging of metabotropic glutamate receptor subtype 5 (mGluR5). Am J Nucl Med Mol Imaging. 2012; 2:29–32. [PubMed: 23133800]
45. Li S, Huang Y. In vivo imaging of the metabotropic glutamate receptor 1 (mGluR1) with positron emission tomography: recent advance and perspective. Curr Med Chem. 2014; 21:113–123. [PubMed: 23992339]
46. Wang J-Q, Kuruppu D, Brownell A-L. Radiosynthesis of the $mGluR_{2/3}$ PET tracer (*S, S, S*)-2-(2-carboxycyclopropyl)-2-(4-[^{11}C]methoxyphenethyl)glycine dimethyl ester ([^{11}C]CMG). J Nucl Med. 2008; 49:286P.
47. Wang J-Q, Zhang Z, Kuruppu D, Brownell A-L. Radiosynthesis of PET radiotracer as a prodrug for imaging group II metabotropic glutamate receptors in vivo. Bioorg Med Chem Lett. 2012; 22:1958–1962. [PubMed: 22318160]
48. Celen S, Koole M, Alcazar J, De Angelis M, Schmidt M, Van Laere K, Verbruggen A, Langlois X, Andres JI, Bormans G. Preliminary biological evaluation of [^{11}C]JNJ42491293 as a radioligand for PET imaging of $mGluR_2$ in brain. J Nucl Med. 2012; 53:286.
49. Andrés J-I, Alcázar J, Cid JM, De Angelis M, Iturrino L, Langlois X, Lavreysen H, Trabanco AA, Celen S, Bormans G. Synthesis, Evaluation, and Radiolabeling of New Potent Positive Allosteric Modulators of the Metabotropic Glutamate Receptor 2 as Potential Tracers for Positron Emission Tomography Imaging. J Med Chem. 2012; 55:8685–8699. [PubMed: 22992024]
50. Majo V, Prabhakaran J, Simpson N, Arango V, Mann JJ, Kumar JD. Development of a [^{18}F]-labeled positive allosteric modulator of the metabotropic glutamate receptor 2 ($mGluR_2$) as a potential PET tracer. J Nucl Med. 2013; 54:1072. [PubMed: 23637201]
51. Ma Y, Kumata K, Yui J, Zhang Y, Yamasaki T, Hatori A, Fujinaga M, Nengaki N, Xie L, Wang H, Zhang M-R. Synthesis and evaluation of 1-(cyclopropylmethyl)-4-(4-[^{11}C]methoxyphenyl)-piperidin-1-yl-2-oxo-1,2-dihydropyridine-3-carbonitrile ([^{11}C]CMDC) for PET imaging of metabotropic glutamate receptor 2 in the rat brain. Bioorg Med Chem. 2017; 25:1014–1021. [PubMed: 28049619]
52. PCT/US2015/046962.
53. WO2016/087489A1.
54. Lavreysen H, Langlois X, Ahnaou A, Drinkenburg W, te Riele P, Biesmans I, Van der Linden I, Peeters L, Megens A, Wintmolders C, Cid JM, Trabanco AA, Andres JI, Dautzenberg FM, Lutjens R, Macdonald G, Atack JR. Pharmacological characterization of JNJ-40068782, a new potent, selective, and systemically active positive allosteric modulator of the mGlu2 receptor and its radioligand [^{3}H]JNJ-40068782. J Pharmacol Exp Ther. 2013; 346:514–527. [PubMed: 23766542]
55. Van Laere K, Koole M, de Hoon J, Van Hecken A, Langlois X, Andres JI, Bormans G, Schmidt M. Biodistribution, dosimetry and kinetic modeling of [^{11}C]JNJ-42491293, a PET tracer for the $mGluR_2$ receptor in the human brain. J Nucl Med. 2012; 53:355.
56. Leurquin-Sterk G, Celen S, Van Laere K, Koole M, Bormans G, Langlois X, Van Hecken A, te Riele P, Alcázar J, Verbruggen A, de Hoon J, Andrés J-I, Schmidt ME. What We Observe In Vivo Is Not Always What We See In Vitro: Development and Validation of ^{11}C-JNJ-42491293, A Novel Radioligand for $mGluR_2$. J Nucl Med. 2017; 58:110–116. [PubMed: 27469358]
57. McQuade P, Joshi A, Miller P, Zeng Z, Purcell M, Gantert L, Holahan M, Meissner R, Uslaner J, Hostetler E. Discovery and Preclinical Evaluation of an $mGluR_2$-NAM PET Radioligand. J Nucl Med. 2016; 57:290.
58. Lohith T, McQuade P, Salinas C, Anderson M, Reynders T, Bautmans A, Bormans G, Serdons K, Van Laere K, Hostetler E. First-in-human PET imaging of $mGluR_2$ receptors. J Nucl Med. 2016; 57:213.
59. WO2013/066736A1.
60. Niswender CM, Johnson KA, Luo Q, Ayala JE, Kim C, Conn PJ, Weaver CD. A novel assay of $G_{i/o}$-linked G protein-coupled receptor coupling to potassium channels provides new insights into

the pharmacology of the group III metabotropic glutamate receptors. Mol Pharmacol. 2008; 73:1213–1224. [PubMed: 18171729]

61. Hemstapat K, Da Costa H, Nong Y, Brady AE, Luo Q, Niswender CM, Tamagnan GD, Conn PJ. A novel family of potent negative allosteric modulators of group II metabotropic glutamate receptors. J Pharmacol Exp Ther. 2007; 322:254–264. [PubMed: 17416742]
62. Kroeze WK, Sassano MF, Huang XP, Lansu K, McCorvy JD, Giguere PM, Sciaky N, Roth BL. PRESTO-Tango as an open-source resource for interrogation of the druggable human GPCRome. Nat Struct Mol Biol. 2015; 22:362–369. [PubMed: 25895059]
63. Arunlakshana O, Schild HO. Some quantitative uses of drug antagonists. Br J Pharmacol Chemother. 1959; 14:48–58. [PubMed: 13651579]
64. Waterhouse RN. Determination of lipophilicity and its use as a predictor of blood-brain barrier penetration of molecular imaging agents. Mol Imaging Biol. 2003; 5:376–389. [PubMed: 14667492]
65. Patel S, Gibson R. In vivo site-directed radiotracers: a mini-review. Nucl Med Biol. 2008; 35:805–815. [PubMed: 19026942]
66. Pike VW. Considerations in the Development of Reversibly Binding PET Radioligands for Brain Imaging. Curr Med Chem. 2016; 23:1818–1869. [PubMed: 27087244]
67. OECD. Test No. 107: Partition Coefficient (n-octanol/water): Shake Flask Method. OECD Publishing;
68. Chung, TDY., Terry, DB., Smith, LH. In Vitro and In Vivo Assessment of ADME and PK Properties During Lead Selection and Lead Optimization - Guidelines, Benchmarks and Rules of Thumb. Bethesda (MD): Eli Lilly & Company and the National Center for Advancing Translational Sciences; 2015. 2004-
69. Gill SS, Pulido OM. Glutamate receptors in peripheral tissues: current knowledge, future research, and implications for toxicology. Toxicol Pathol. 2001; 29:208–223. [PubMed: 11421488]
70. Andrés J-I, Alcázar J, Cid JM, De Angelis M, Iturrino L, Langlois X, Lavreysen H, Trabanco AA, Celen S, Bormans G. Synthesis, Evaluation, and Radiolabeling of New Potent Positive Allosteric Modulators of the Metabotropic Glutamate Receptor 2 as Potential Tracers for Positron Emission Tomography Imaging. J Med Chem. 2012; 55:8685–8699. [PubMed: 22992024]
71. Johnson BG, Wright RA, Arnold MB, Wheeler WJ, Ornstein PL, Schoepp DD. [^{3}H]-LY341495 as a novel antagonist radioligand for group II metabotropic glutamate (mGlu) receptors: characterization of binding to membranes of mGlu receptor subtype expressing cells. Neuropharmacology. 1999; 38:1519–1529. [PubMed: 10530814]
72. Nikiforuk A, Popik P, Drescher KU, van Gaalen M, Relo AL, Mezler M, Marek G, Schoemaker H, Gross G, Bespalov A. Effects of a positive allosteric modulator of group II metabotropic glutamate receptors, LY487379, on cognitive flexibility and impulsive-like responding in rats. J Pharmacol Exp Ther. 2010; 335:665–673. [PubMed: 20739457]
73. Harpsoe K, Isberg V, Tehan BG, Weiss D, Arsova A, Marshall FH, Brauner-Osborne H, Gloriam DE. Selective Negative Allosteric Modulation Of Metabotropic Glutamate Receptors - A Structural Perspective of Ligands and Mutants. Sci Rep. 2015; 5:13869. [PubMed: 26359761]
74. Lundström L, Bissantz C, Beck J, Wettstein JG, Woltering TJ, Wichmann J, Gatti S. Structural determinants of allosteric antagonism at metabotropic glutamate receptor 2: mechanistic studies with new potent negative allosteric modulators. Br J Pharmacol. 2011; 164:521–537. [PubMed: 21470207]
75. Rydberg P, Gloriam DE, Zaretzki J, Breneman C, Olsen L. SMARTCyp: A 2D Method for Prediction of Cytochrome P450-Mediated Drug Metabolism. ACS Medicinal Chemistry Letters. 2010; 1:96–100. [PubMed: 24936230]
76. Tatsuta T, Naito M, Oh-hara T, Sugawara I, Tsuruo T. Functional involvement of P-glycoprotein in blood-brain barrier. J Biol Chem. 1992; 267:20383–20391. [PubMed: 1356979]
77. Pike VW. PET Radiotracers: crossing the blood-brain barrier and surviving metabolism. Trends Pharmacol Sci. 2009; 30:431–440. [PubMed: 19616318]
78. Wang L, Yui J, Wang Q, Zhang Y, Mori W, Shimoda Y, Fujinaga M, Kumata K, Yamasaki T, Hatori A, Rotstein BH, Collier TL, Ran C, Vasdev N, Zhang M-R, Liang SH. Synthesis and

preliminary PET imaging studies of a FAAH radiotracer ([^{11}C]MPPO) based on α-ketoheterocyclic scaffold. ACS Chem Neurosci. 2016; 7:109–118. [PubMed: 26505525]

79. Wang L, Mori W, Cheng R, Yui J, Hatori A, Ma L, Zhang Y, Rotstein BH, Fujinaga M, Shimoda Y, Yamasaki T, Xie L, Nagai Y, Minamimoto T, Higuchi M, Vasdev N, Zhang M-R, Liang SH. Synthesis and Preclinical Evaluation of Sulfonamido-based [^{11}C-*Carbonyl*]-Carbamates and Ureas for Imaging Monoacylglycerol Lipase. Theranostics. 2016; 6:1145–1159. [PubMed: 27279908]
80. Sidique S, Dhanya R-P, Sheffler DJ, Nickols HH, Yang L, Dahl R, Mangravita-Novo A, Smith LH, D'Souza MS, Semenova S, Conn PJ, Markou A, Cosford NDP. Orally Active Metabotropic Glutamate Subtype 2 Receptor Positive Allosteric Modulators: Structure-Activity Relationships and Assessment in a Rat Model of Nicotine Dependence. J Med Chem. 2012; 55:9434–9445. [PubMed: 23009245]
81. Dhanya RP, Sheffler DJ, Dahl R, Davis M, Lee PS, Yang L, Nickols HH, Cho HP, Smith LH, D'Souza MS, Conn PJ, Der-Avakian A, Markou A, Cosford ND. Design and synthesis of systemically active metabotropic glutamate subtype-2 and -3 (mGlu2/3) receptor positive allosteric modulators (PAMs): pharmacological characterization and assessment in a rat model of cocaine dependence. J Med Chem. 2014; 57:4154–4172. [PubMed: 24735492]
82. Wang L, Mori W, Cheng R, Yui J, Hatori A, Ma L, Zhang Y, Rotstein BH, Fujinaga M, Shimoda Y, Yamasaki T, Xie L, Nagai Y, Minamimoto T, Higuchu M, Vasdev N, Zhang M-R, Liang SH. Synthesis and Preclinical Evaluation of Sulfonamido-based [^{11}C-Carbonyl]-Carbamates and Ureas for Imaging Monoacylglycerol Lipase. Theranostics. 2016; 6:1145–1159. [PubMed: 27279908]
83. Reed, GA. Curr Protoc Pharmacol. Vol. 75. John Wiley & Sons, Inc; 2016. Stability of Drugs, Drug Candidates, and Metabolites in Blood and Plasma; p. 7.6.1-7.6.12.
84. Hill JR. In vitro drug metabolism using liver microsomes. Curr Protoc Pharmacol. 2004; 23:7.8:7.8.1–7.8.11.

ABBREVIATIONS

PET	positron emission tomography
mGlu$_2$	metabotropic glutamate receptor 2
PAM	positive allosteric modulator
NAM	negative allosteric modulator
NBS	*N*-bromosuccinimide
AIBN	2,2-azobis(2-methylpropionitrile)
mCPBA	*meta*-chloroperbenzoic acid
DCM	dichloromethane
DMF	dimethylformamide
ADME	absorption, distribution, metabolism and excretion
MPO	multiparameter optimization
SUV	standardized uptake value
TAC	time-activity curve
%ID/g	percentage of injected dose per gram of wet tissue
KO	knockout

PgP P-glycoprotein

Bcrp breast cancer resistance protein.

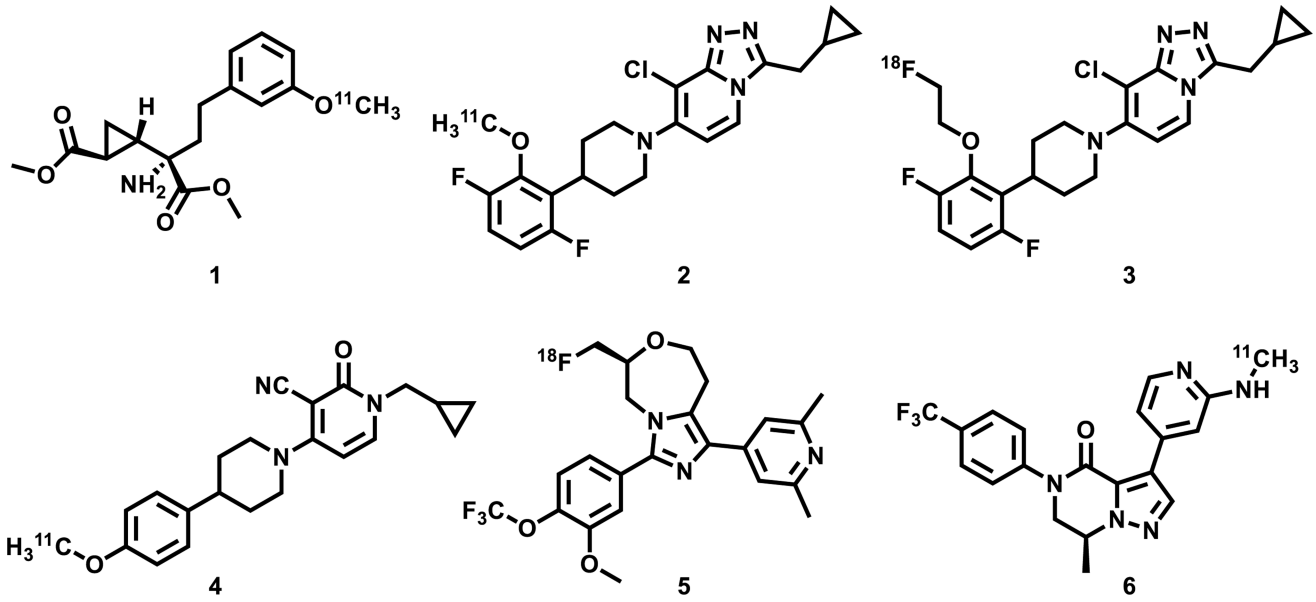

Figure 1.

PET tracers targeting $mGlu_2$. While the majority of compounds in this figure have no selectivity data available in the primary literature, compound **2** showed $mGlu_2$ selectivity greater than 350 fold over the other mGlu receptors.[49]

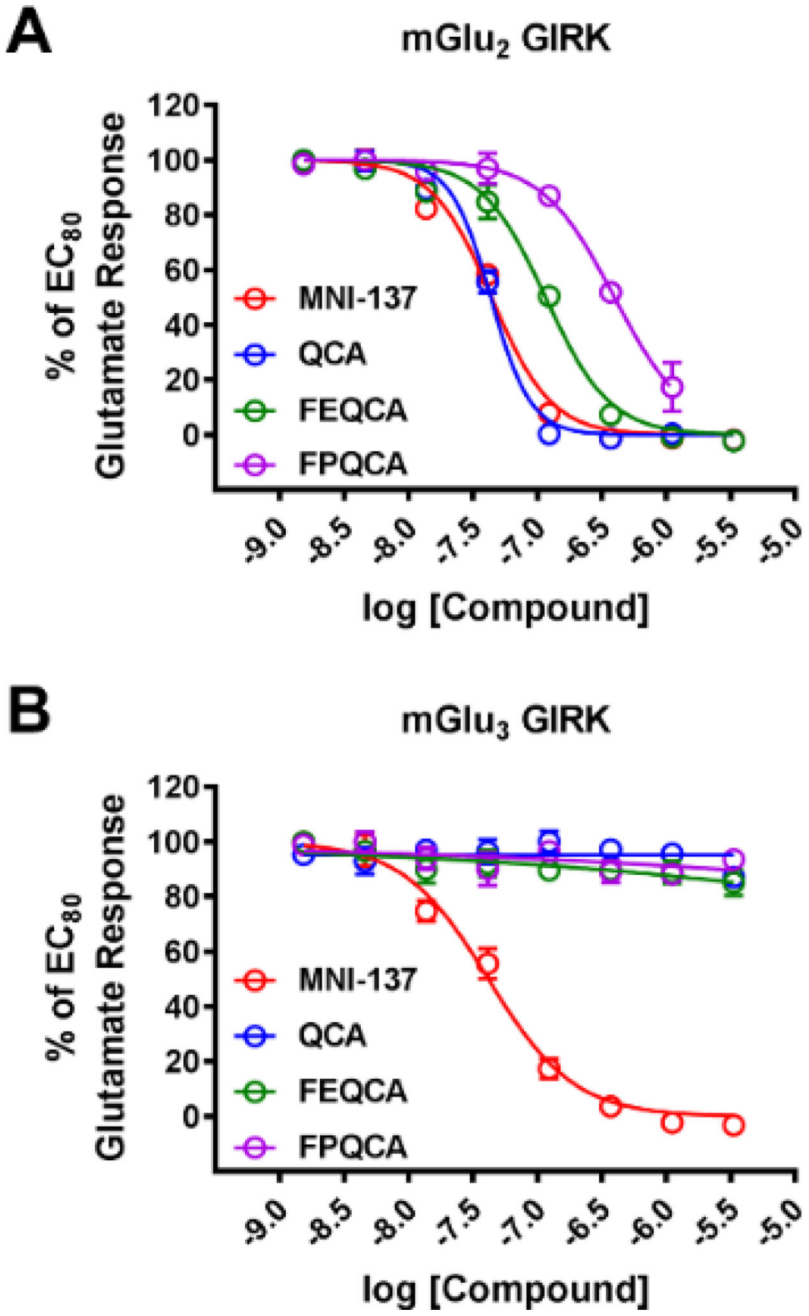

Figure 2.

In vitro evaluation of the potencies of QCA, FEQCA, FPQCA, and the control $mGlu_{2/3}$ NAM MNI-137 in $mGlu_2$ GIRK (A) or $mGlu_3$ GIRK (B) functional assays.

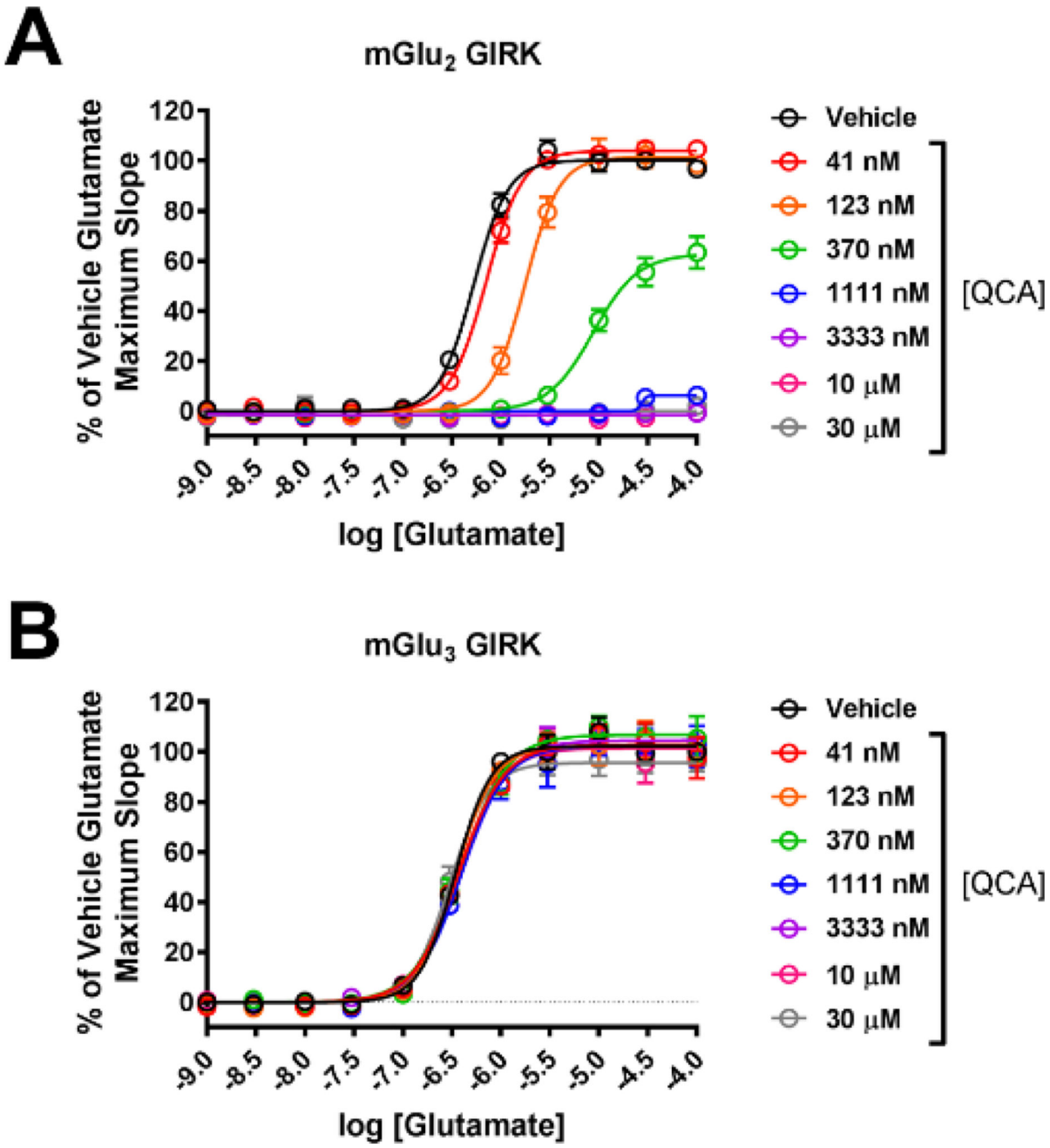

Figure 3.

QCA noncompetitively right-shifts the glutamate concentration-response for $mGlu_2$ and decreases the maximal glutamate response (A) but has no effect on the glutamate concentration-response for $mGlu_3$ (B).

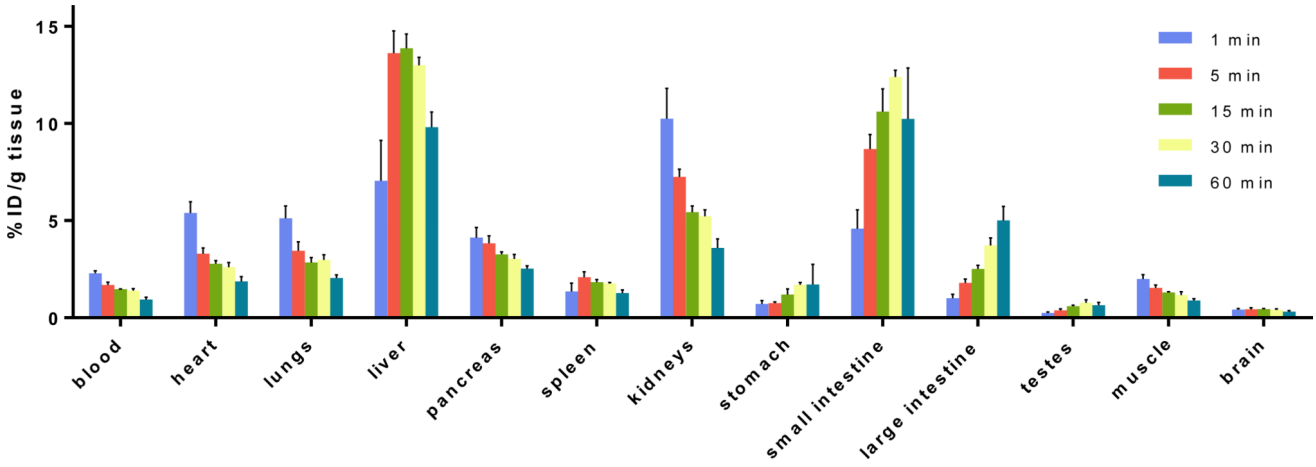

Figure 4.

Ex vivo biodistribution in mice at five different time points (1, 5, 15, 30 and 60 min) post [^{11}C]QCA injection. Data are expressed as %ID/g.

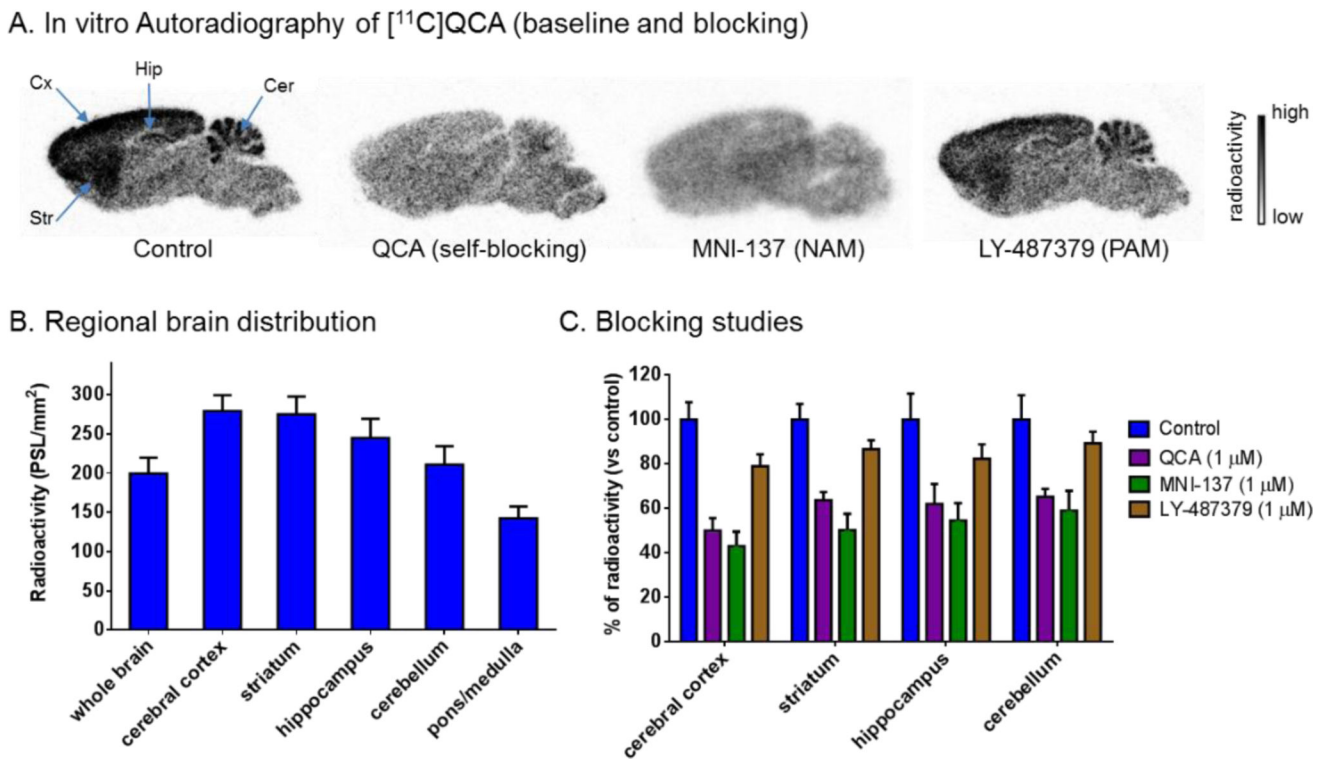

Figure 5.

In vitro autoradiography of [^{11}C]QCA binding in rat brain sections. (A) Brain sections were treated with [^{11}C]QCA in the absence (baseline) or presence of QCA, MNI-137, LY-487379 (1 μM each). Cer, cerebellum; Hip, hippocampus; Cx, cortex; Str, striatum. (B) The radioactivity distribution was quantified in regional rat brain. The data are expressed as radioactivity per mm^2 (n = 4). (C) Blocking studies. The data are normalized to % of radioactivity vs control (n = 4).

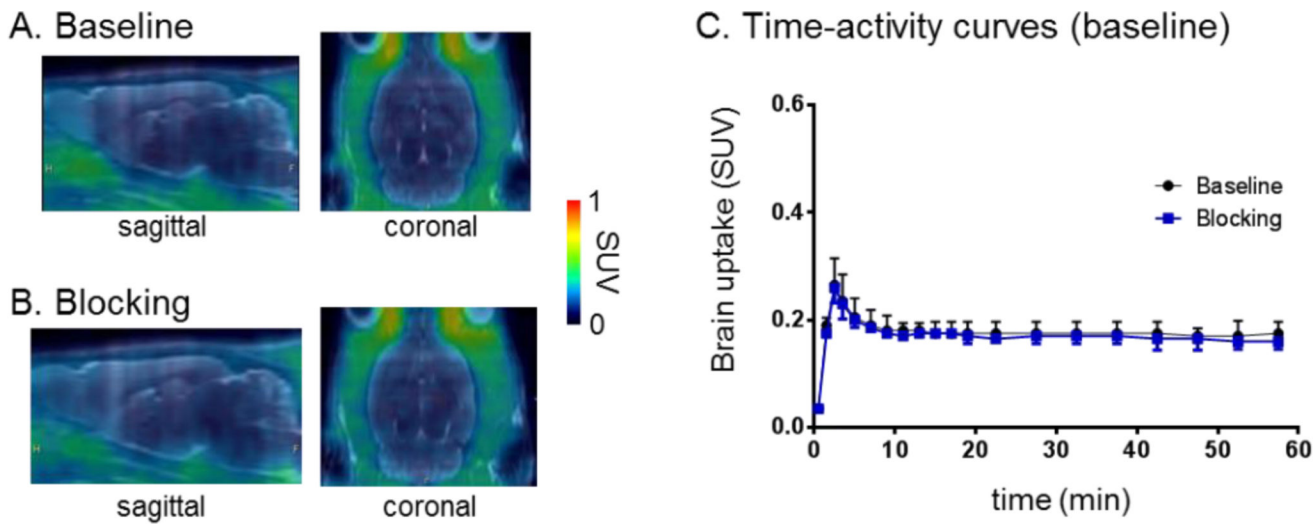

Figure 6.

PET/MRI fused images of [^{11}C]QCA in rat brain: (A) baseline and (B) self-blocking with QCA (1 mg/kg). (C) Time-activity curves in whole brain under baseline and QCA self-blocking.

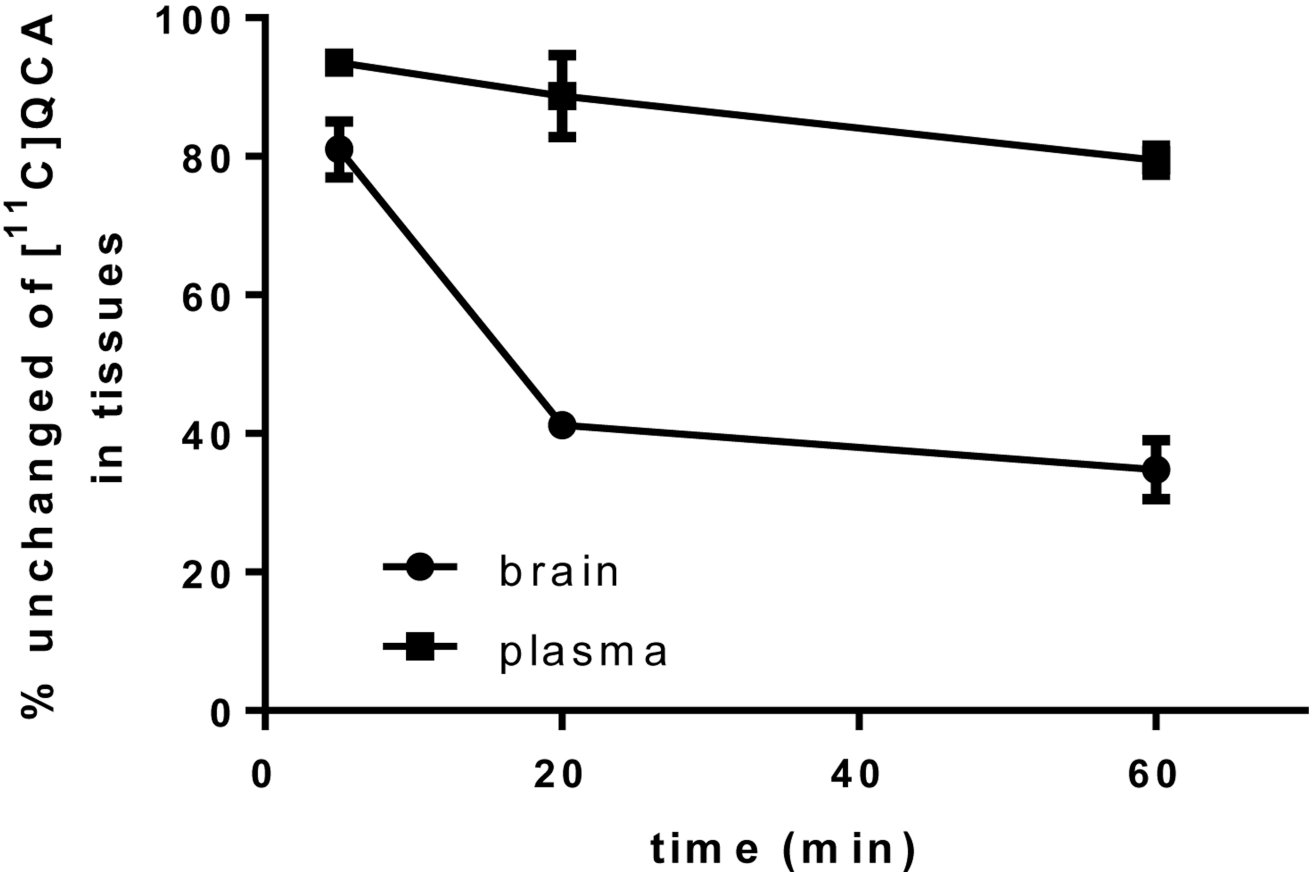

Figure 7.
Percentages of unchanged [^{11}C]QCA in rat brain tissue and plasma (n = 3) at 5, 20 and 60 min post injection.

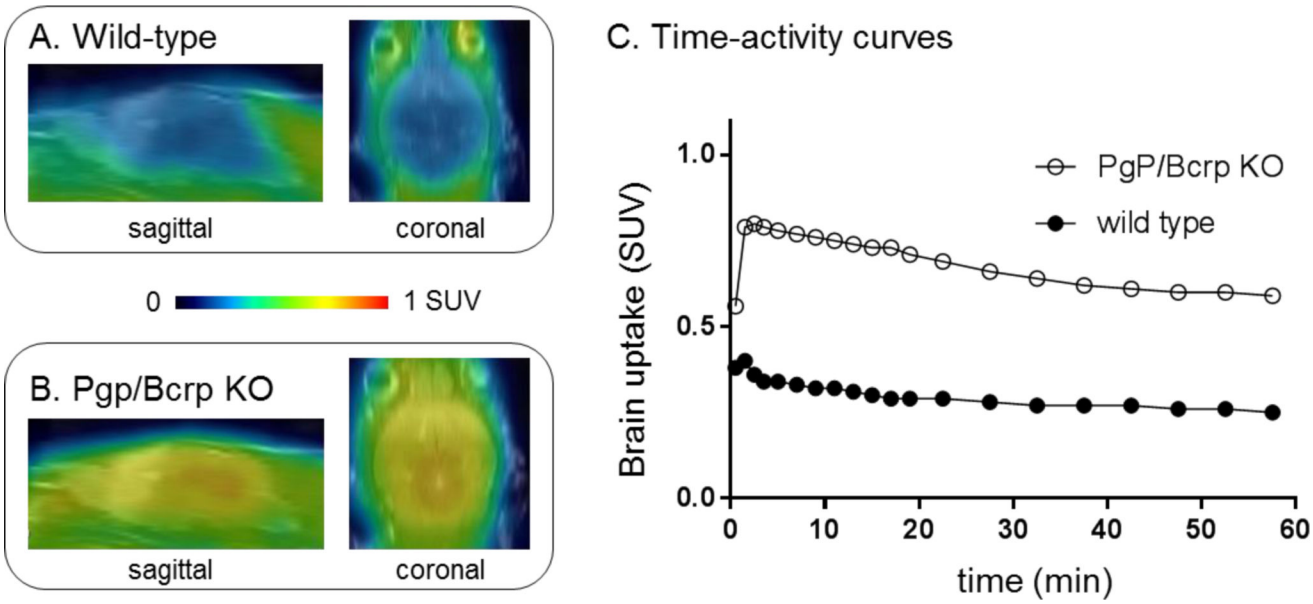

Figure 8.

PET/MRI fused images in the whole brain of (A) wild-type and (B) Pgp/Bcrp knockout mouse. (C) Time-activity curves of whole brain in wildtype and Pgp/Bcrp knockout mouse after [^{11}C]QCA injection.

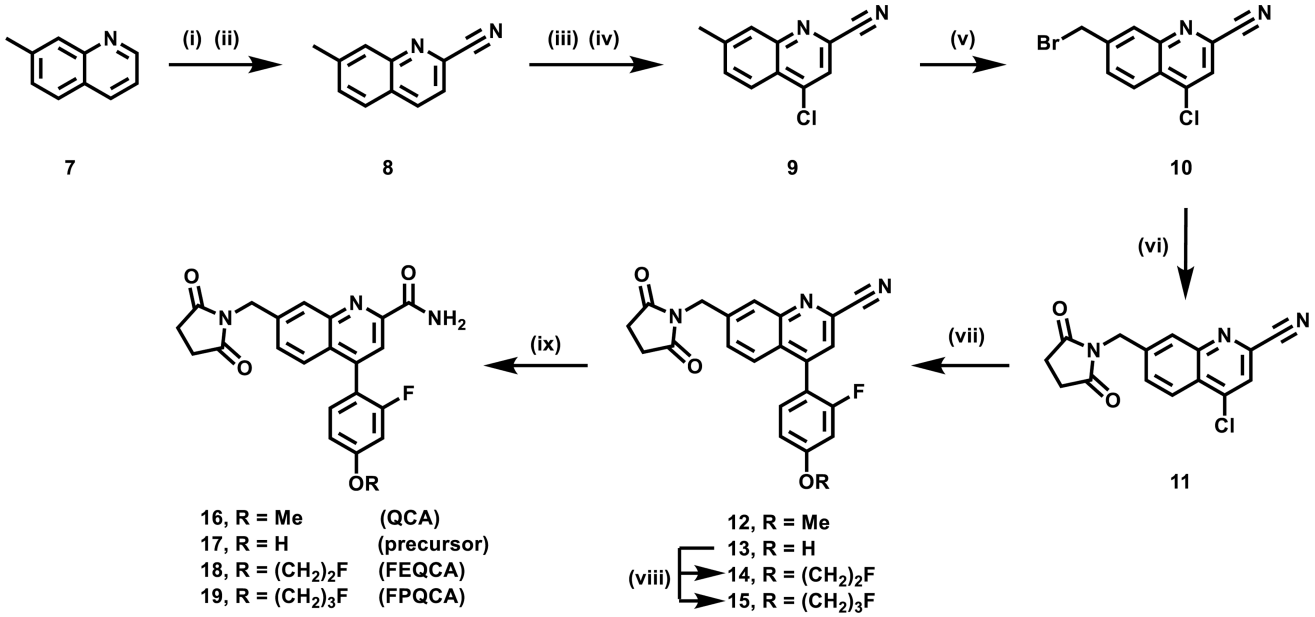

Scheme 1.

Synthesis of quinoline 2-carboxamide analogs. (i) *m*CPBA, DCM, 1h; (ii) TMSCN, dimethylcarbamic chloride, DCM, 12 h, 74% for two steps; (iii) *m*CPBA, DCM, 40°C, 4 h; (iv) $POCl_3$, DMF, $CHCl_3$, 70°C, 6 h, 64% yield for two steps; (v) NBS, Benzoyl peroxide, CCl_4, 85°C, 4 h, 60% yield; (vi) succinimide, Cs_2CO_3, DMF, 30 min, 80% yield; (vii) arylboronic acid, $Pd(PPh_3)_4$, Na_2CO_3, 1,4-dioxane, H_2O, 100°C; (viii) Cs_2CO_3, DMF, 12 h, IC_2H_4F for **14**, 45% yield over 2 steps from **11**; IC_3H_6F for **15**, 53% yield over 2 steps from **11**; (ix) sodium percarbonate, 55% yield for QCA (**16**) over 2 steps from **11**, 51% yield for precursor **17** over 2 steps from **11**, 60% yield for FEQCA (**18**), and 53% yield for FPQCA (**19**).

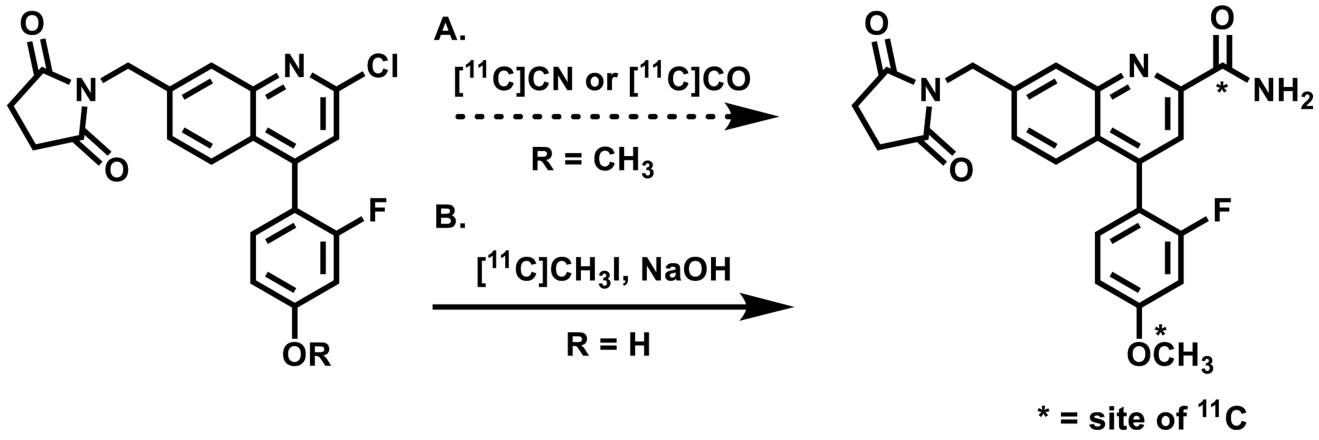

Scheme 2.

Radiosynthesis of [^{11}C]QCA (A) potential labeling methods; (B) $^{11}CH_3I$ labeling method.

Table 1

Physicochemical properties of QCA (**16**), FEQCA (**18**) and FPQCA (**19**).

Entry	lipophilicity[a]		pH stability[b]			plasma stability[c]	microsomal stability[d]
	cLogP	LogP	5.0	7.4	9.4		
16	2.95	1.27	97.9%	50.9%	46.7%	22.5%	64.4%
18	3.44	1.75	98.5%	53.6%	59.0%	46.7%	70.1%
19	3.69	1.99	91.5%	72.5%	76.3%	87.5%	64.6%

[a]lipophilicity is calculated and measured by Pallas 3.0 software and the shake flask method, respectively.

*b–d*percent (average, n ≥ 3) remaining of the parent molecule after incubation at 37 °C for 60 min.

[c]diltiazem and

[d]verapamil as positive controls, respectively.